Trinity College Dublin
Coláiste na Tríonóide, Baile Átha Cliath
The University of Dublin

The implementation of air curtains on realistic aircraft nose and main landing gear

Charlotte Meuly

Supervisor: Prof. Gareth Bennett

Department of Mechanical, Manufacturing & Biomedical Engineering
School of Engineering
Trinity College Dublin, *the University of Dublin*
D02 PN40
Ireland

August 2022

A dissertation submitted to the University of Dublin in partial fulfilment of the requirements for the degree of MSc.

Declaration

I agree that this thesis was completed in line with the plagiarism provisions in the General Regulations of the University Calendar for the current year, found at http://www.tcd.ie/calendar.

I have completed the Online Tutorial on avoiding plagiarism 'Ready Steady Write', located at http://tcd-ie.libguides.com/plagiarism/ready-steady-write.

I agree that this thesis will not be publicly available but will be available to TCD staff and students in the University's open access institutional repository on the Trinity domain only.

Charlotte Meuly, November 2021

Acknowledgements

I would like to thank Professor Gareth Bennett, for trusting me with this research project. His guidance was most helpful in understanding the complex topic of noise in aviation, as well as the methods and tools used during this year.

I would also like to thank my friend Richard Lagrée, for his support and skills in 3D CAD modelling and FDM 3D-printing. He designed and printed many parts for the preliminary tests, and gave me the explanations needed to continue his work on the CAD models.

I would like to thank Eoghan Ross, for teaching me how to use the SLA printer, and for his patience and help when I did my prints.

I would like to thank Professor Tim Persoons and Professor John Kennedy, for lending me hot-wire probes and a sound-level meter, and for teaching me how to best use them.

Finally, I wish to thank my friends and my family, for their kind support during this year.

Contents

List of Figures

List of Tables

Nomenclature

Acronyms

ALLEGRA Advanced Low Noise Landing Gear for Regional Aircraft

CAA Computational AeroAcoustics

CFD Computational Fluid Dynamics

CTA Constant Temperature Anemometry

DAS Data Acquisition System

DLR German Aerospace Center

EPNL Effective Perceived Noise Level

HWA Hot-Wire Anemometry

ICAO International Civil Aviation Organisation

INVENTOR INnovative dEsign of iNstalled airframe componenTs for aircraft nOise Reduction

LNT Low-Noise Technology

MLG Main Landing Gear

NLG Nose Landing Gear

PIV Particule Image Velocimetry

SLM Sound-Level Meter

TRL Technology Readiness Level

WHO World Health Organisation

Chapter 1

Introduction

1.1 Context and Research Motivation

The aviation sector is a pillar of global economy, transporting people and goods across the planet at the highest speed. As a result, more than 38 millions of flights took place in 2019, after years of steady increase in air traffic [6]. Having taken a recent hit with Covid-19, air traffic is now picking up again. Airports' capacities are increased, with a renewed interest from the low-cost companies in smaller airports. For example, traffic significantly increased at Paris Beauvais airport in 2004 with the arrival of low cost companies, jumping from 423,520 flights in 2002 to 1,427,595 flights in 2004 [7]. Despite being called "Paris Beauvais airport", it is more than an hour drive from Paris city center. The airport is actually very close by to a small village in northern France.

This change in traffic volume has been under scrutiny by researchers from all fields: biodiversity [8, 9], health [10], environmental studies [11]... The influence of aircraft noise on population has been particularly studied. Possible correlations between health issues and aircraft noise exposure are explored in many research papers. The World Health Organisation (WHO) [12] provides guidelines for European legislation on harmful noise exposure, based on peer-reviewed evidences [13, 14]. Noise exposure can alter sleep, affect mental health, and a link has recently been established with cardiovascular diseases [15, 16]. Aircraft noise reduction is a current challenge that could have an impact on many. In the case of small airports with increasing air traffic, like Paris Beauvais, reducing noise would most certainly be very beneficial to close-by communities.

Noise from air traffic can be divided in two sources: engine noise and airframe noise. Engine noise was the main source in aviation's early days, especially during take-off and landing. In the 1970's, there has been a change in engine technology, from turbojets to turbofans. When turbojets rejected air at a very high speed, compared to the ambient air flow, turbofans have a portion of the incoming flow by-passing the engine, creating a layer of air at intermediate speed between the engine flow and the ambient flow [17]. The flow velocity difference is therefore lessened and produces less noise. With current aircrafts, engine noise and airframe noise are in comparable proportions [1].

Airframe noise comes from the modification of the shape of the plane in order to lift the plane during take-off, or to slow down during landing. The aircraft is positioned against the

ambient airflow, creating more friction and inducing a higher noise level. A great proportion of the airframe noise comes from the landing gear. The landing gear is a highly technical set of tubes and junctions, designed to support very high loads during take-off and landing. Its current shape is not aerodynamic and causes flow separation and turbulent flow. Due to security requirements, as well as specifications on weight and volume, the landing gear has never really been modified, in spite of its high contribution to noise generation. Some technologies have been explored to protect the landing gear from the incoming air flow, such as fairings and meshes, but failed to be put into place [18].

In this report, another technology is considered, named "air curtains". These air curtains consist in planar jets placed before the landing gear, perpendicularly to the ambient flow. The air coming out of the jets shields the landing gear from the ambient flow, deflecting the incoming air which usually produces the noise [5]. Several geometries have been envisaged [19, 20]: shielding the wheels, the struts, the whole landing gear... Up to now, the air curtain technology already showed encouraging results in shielding bluff bodies, limiting air velocity and reducing noise at certain frequencies. This report focuses on tests to characterise the impact of air curtains on scaled-down landing gears.

1.2 Scope and Research Objectives

The overarching objective of the research was to contribute to the development of an air curtain technology that can reduce the aerodynamic noise radiated from aircraft landing gear noise. Tools and methods were developed, and were/will be implemented in two test campaigns scheduled within the EU funded H2020 collaborative project: INVENTOR (INnoVative dEsign of iNstalled airframe componenTs for aircraft nOise Reduction) [21]. Objectives were set for the whole project and the detailed aims and skills required to achieve these objectives are listed.

1.2.1 Aims

The global objectives for the aforementioned test campaigns were the following:

- To develop suitable air curtain systems for a scaled model Lagoon Nose Landing Gear (NLG) mounted on a flat plate to be tested in DLR, the German Aerospace Center, in February 2022.

- To develop suitable air curtain systems for a scaled model Lagoon NLG mounted within a Dassault designed wing section also to be tested in DLR in February 2022.
- To investigate the adaptability of these air curtains for a scaled model generic business jet trailing arm Main Landing Gear (MLG) mounted within a Dassault designed wing section to be tested in DLR.

In order to achieve these objectives, the following tools, techniques, and methods needed to be developed. Both experimental and numerical methods were used.

- Develop skills in fluid flow control, regulation and measurement systems, including hot-wire anemometry and Pitot-static velocity analysis.
- Develop skills in FDM and MSLA 3D printing to facilitate air curtain design for prototyping and evaluation.
- Design and build a rig to support the air curtain designs for cross-flow evaluation mounted to an existing open-jet wind tunnel.
- (Re)design and implement a hot-wire traverse system to characterise the air flow of the nozzle outlet and the air curtain trajectory in both quiescent and in cross-flow conditions.
- Implement identical geometries in a numerical environment for CFD analysis using Ansys Fluent.
- Develop numerical analysis skills to predict the flow's behaviour, correct air curtains' designs and compare flow velocity and distribution in identical boundary conditions.
- Contribute to the data analysis of both experimental and numerical results.
- Develop skills in Latex and Zotero.
- Write a literature review on the topic of airframe noise reduction.

Chapter 2

Literature Review

2.1 Background

2.1.1 Noise in aviation

After World War II, there has been a great boom in civil aviation, with a massive increase in number of flights, reaching more than 38 millions of flights in 2018 for the airline industry [6]. Such increase in air traffic resulted in an equally important increase in aircraft noise pollution. When typing in "aircraft noise pollution", the earliest research papers on the subject were written in the 1960's. Papers at the time mentioned turbines as the main source of noise [22] and already studied the impact of noise on human health. Research points out possible link between aircraft noise exposure and children's learning capabilities, negatively impacting their ability to read, concentrate and memorise [10]. The same review also mentions the effect of transportation noise on sleep. Regular exposure to aviation noise during night time can lead to sleep disruption, awakenings, and disturbed sleep cycles. WHO recently reviewed the quality of the evidence on the effects of noise exposure on sleep [14]. Sleep disturbance can increase the chance to develop cardiovascular diseases, such as arrhythmia or arterial hypertension. Studies have looked at potential correlations with such diseases and aviation noise exposure [15]. Because of situational and individual moderators, reviews often conclude that more studies need to be conducted to be able to strongly affirm the correlation between aircraft noise and altered health conditions. Even though further studies are needed, noise is regularly mentioned as a source of annoyance and has an effect on people's well-being [13, 16].

In the 1960's, supersonic technology was developed, which produced more noise and pollution for surrounding populations, resulting in a call for increased control of plane noise generation [23]. International standards were therefore implemented in 1971. The International Civil Aviation Organization (ICAO) defines a standard in Annex 16, Vol.1 [24]. This standard has been adapted by the Federal Aviation Administration (FAA) in Part 36 for the US. To make sure that planes respect ICAO's standard, they go through a standardised test in order to measure the Effective Perceived Noise Level (EPNL). At predetermined positions near landing and take-off sites, the EPNL cannot be higher than 108 EPNLdB [25].

Several governmental programs have recently been put into place to research ways to reduce aircraft noise. In the US, the Aviation Sustainability CENTer (ASCENT), funded among others by the FAA and NASA, is in charge of research for a more sustainable avi-

ation industry. Noise reduction is mentioned as one of the goals for Next Generation Air Transportation System [26]. Other programs such as NASA program Advanced Air Transport Technology (AATT) cite noise reduction among their objectives for a cleaner and more efficient aviation. AATT program is about exploring very early-stage technologies that could be implemented in quite a while, "2035-2045" [27]. Such programs also take place in Europe; the Advisory Council for Aviation Research and Innovation (ACARE) has defined a Strategic Research and Innovation Agenda (SRIA) with long-term objectives regrouped under the name FlightPtah 2050. One of them mentions the objective to reduce by 65% noise emissions, compared to a typical aircraft in 2000 [28]. It's with these objectives in mind that the INVENTOR program was established to look at solutions to reduce airframe noise during approach and landing.

2.1.2 Noise sources

Airframe noise is one of the two types of noise encountered with an airplane. It is defined as the noise generated by the airflow on the aircraft structure. Some shapes are particularly responsible for the generation of noise such as trailing edges, holes or bluff bodies. All these shapes induce mixing of flows with different pressures, creation of shedding vortexes and turbulent behaviours. All of these result in an increase in noise emissions. These emissions are accentuated when the shape of the plane is modified during take-off and landing, in order to increase either lift or drag. The landing gear is an additional source of airframe noise during these two phases.

The other type of noise is engine noise. It is a result of the great difference in velocity between the combustion gas leaving the engine and the ambient air flow. The high velocity mix of combustion gas and air coming out of the engine generates a turbulent zone along its shear layer, which generates noise. This noise emission was particularly important when aircraft used turbojet engines [29], see Fig. 2.1(a). With this technology, high velocity exhaust flow exiting the nozzle came directly in contact with slower surrounding air flow and generated high noise level. The integration of high-bypass ratio turbofans in aviation resulted in a more efficient propulsion system as well as a quieter technology. The high bypass ratio means that part of the inlet flow doesn't go through the engine and the combustion chamber but is accelerated around the core jet engine, see Fig. 2.1(b). As a result, the core engine outlet flow has a very high velocity. This outlet flow is surrounded by a layer of lower

velocity flow that bypassed the engine. The bypass flow acts as an intermediate-velocity flow between the engine outlet and the ambient flow, actively reducing the turbulence and the noise produced [30].

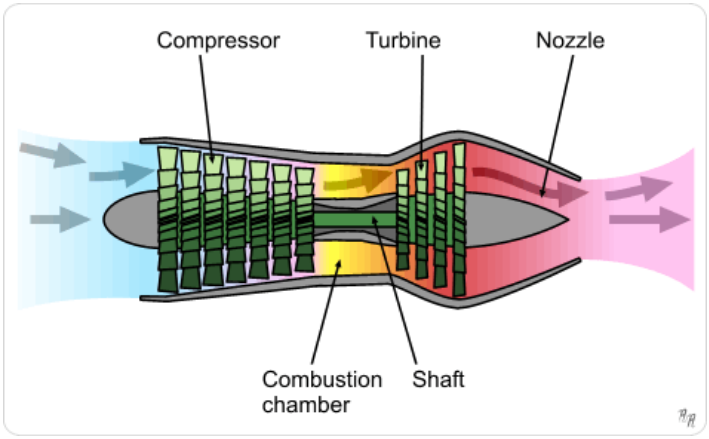

(a) Turbojet configuration

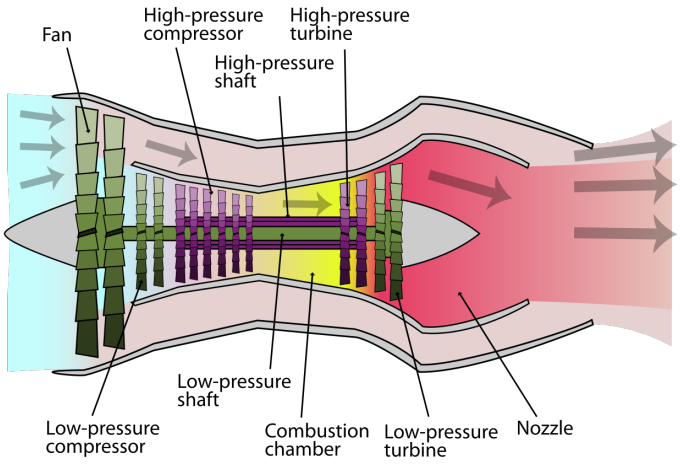

(b) Turbofan configuration

Figure 2.1: Schematics describing turbojet and turbofan configurations, showing the different airflow paths (source: Wikipedia)

This switch from turbojet engines to turbofans had an impact on efficiency, fuel consumption and noise generation. When engines were the dominant source of noise in the first years of aviation, airframe is now as much an important source of noise as engines, as illustrated in Fig. 2.2. This shift in balance has brought to light a new area of focus for research in aviation noise reduction technologies [1]. As seen in Fig. 2.2, within the airframe noise, the landing gear is responsible for a large portion of the noise generated. It has therefore been an focus point of many research papers on airframe noise reduction.

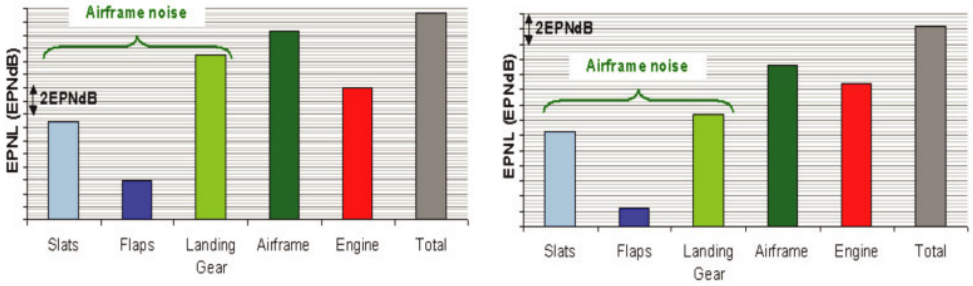

(a) Long range aircraft (b) Short range aircraft

Figure 2.2: Aircraft noise source breakdown at approach (source: Airbus) [1]

2.1.3 Landing gear and noise emissions

The landing gear is composed of several cylinders, side struts, tires, also doors and a cavity, as can be seen in Fig. 2.3.

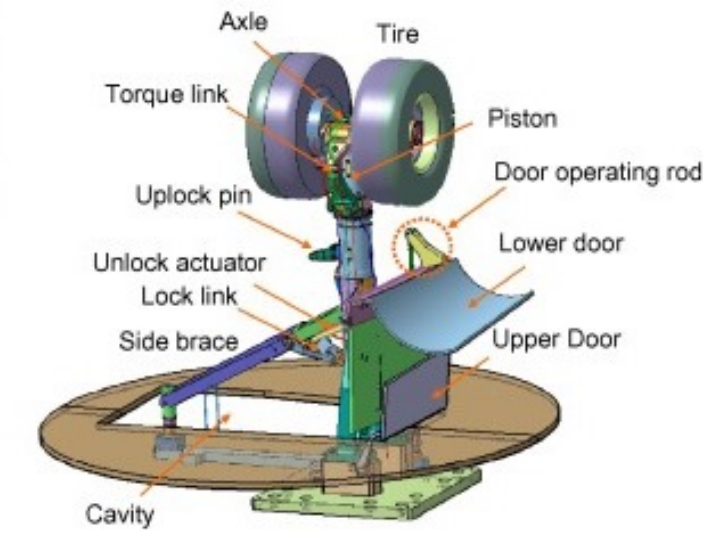

Figure 2.3: Example of a two-wheel landing gear model [2]

All these geometries are highly non-aerodynamic and generate flow separation and reattachment, differences in pressure, turbulence and therefore noise. Even though these structures produce noise in great proportion, the design of the landing gear has not changed for many years due to the following factors:

- Priority on mechanical properties and security: The landing gear is subject to great loads during take-off and landing, in addition to an important air flow. Any modification of the landing gear would mean going through a wide range of tests to ensure that the aircraft's strength and security are not affected.

- Specifications on weight and volume: Aviation requires structures as light as possible to remain efficient. For landing gears in particular, the volume allowed in the casings has been reduced to a minimum. Any noise reduction technology that would require more volume or add weight would hardly be implementable. Technologies that could potentially impede the landing gear deployment, or could disrupt the functionality of other aircraft elements, often fail to reach high Technology Readiness Levels (TRLs).

- Demanding maintenance protocols: Noise reduction technologies implemented around landing gear should not make maintenance more difficult and render visual verification impossible.

- Economic constraints: Any technology that would bring significantly higher costs (higher fuel consumption, more maintenance downtime...) could fail to convince on a commercial level. In the same way, expensive tests and validations can slow down the development of noise reduction technologies for aviation.

2.1.4 Noise prediction

Knowing the complexity of altering the landing gear design, research has been conducted on technologies to reduce noise pollution. Different approaches exist when it comes to predicting the impact of new technologies and the resulting noise levels.

Empirical noise prediction

Some researchers have focused on establishing models that would help predict noise emission and propagation from an aircraft. For example, it has been the objective of NASA's Aircraft NOise Prediction Program (ANOPP). Now at its second iteration, the ANOPP2 software compiles data from flight conditions and ambient parameters to predict what noise would be generated and how it would be perceived, depending on the propagation and the position of the receptor [31]. While investigating airframe noise, some models break down their analysis by components, calculating the contribution of the wings, the tails, the landing gears and the flaps separately [32]. Noise prediction models have been described by Fink in 1977 [33] and Guo in 2006 [34]. Such models are the result of extensive data analysis on a wide range of aircraft geometries and flying conditions. Studies focusing solely on the landing

gear resulted in models that have been verified by flight tests [32, 35] and by wind tunnel tests [34]. Correlations between noise frequencies and geometries are verified, linking low and medium frequency noise to larger components such as the main struts and the wheels, while high frequency noise is produced by smaller details in the geometries. These empirical prediction models, although rather accurate and verified by tests, have limitations when new geometries are introduced. Models then have to be updated and extended to become more largely applicable.

Numerical noise prediction

Another method to predict noise in aviation is via numerical analysis of airflow. This method uses Computational Fluid Dynamics (CFD) and/or Computational AeroAcoustics (CAA). The same way empirical models aim to represent noise generation and noise propagation, numerical models have to take into account both phenomena. CFD is used for predicting the interaction between the air flow and the plane, therefore focusing on the noise generation. The noise level is not always the outcome of the computational studies. It is often the flow velocity that is represented, see Fig. 2.4 for an example of flow velocity calculated around a landing gear.

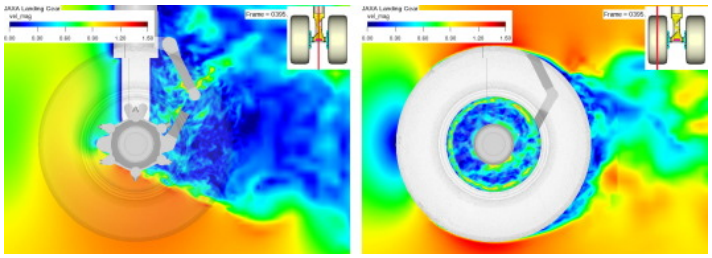

Figure 2.4: Instantaneous velocity magnitude for sections crossing centre of axle and centre of wheel [2]

CAA is then used to study noise propagation, further away from the plane, and to predict the impact on nearby populations for example. Numerical models evolved until finally reaching this hybrid type of studies [36, 37]. As it often is the case for numerical models, the goal is to reach a good compromise. A very fine mesh could yield a more accurate answer but such precision comes at high costs and takes a lot of time. The hybrid CFD/CAA method is widely used as the mesh is very precise where it needs to be (in the near field) while CAA

provides a good approximation of the noise propagation. Such numerical approaches have been used on landing gears [38] and compared to experimental results.

Experimental noise measurement

Experimental noise measurement is the most common approach to noise prediction, as it is often used to verify predictions made using numerical tools or empirical models. There is a wide variety of tests available to characterise either the noise directly or the air flow. Tests can be divided in two parts: flyover tests and wind tunnel tests. During flyover tests, noise level is measured and noise sources are identified. Such tests require extensive microphone arrays and good location tracking of the aircraft to be able synchronise time, noise level and movement. A example of microphone positions during a flyover test is shown in Fig. 2.5. Flyover tests can then be used to verify predictions [35]. The protocol needs to be clearly stated, with a defined set of parameters to describe the landing gears' position, the high lift devices' settings, and the aircraft's speed for example. Flyover tests also require lots of measurements to describe the flight conditions and the airflow (temperature, inflow conditions, ground reflection...).

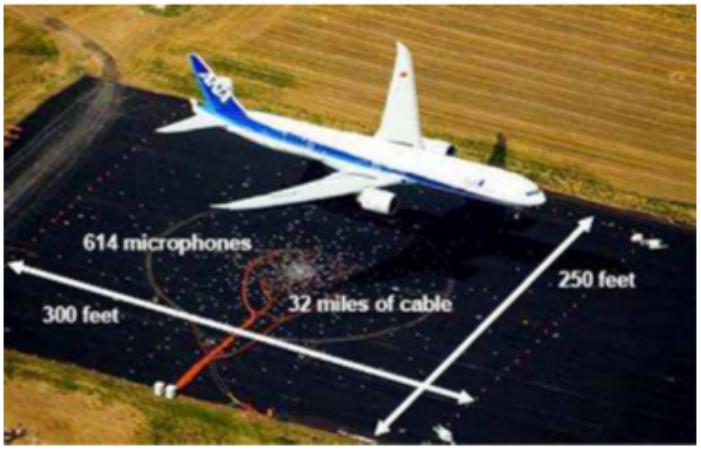

Figure 2.5: Example of a flyover test [3]

Wind tunnels, on the contrary, allow more control over the incoming flow. Experiments in wind tunnels show the interaction between the incoming air and parts of the aircraft. Parts can either be original parts or scaled-down reproductions. In wind tunnels, the noise generated can be measured directly using microphone arrays in anechoic chambers. This means that the noise perceived by the microphones during these tests comes directly from

the air/part interaction, and all noise reflections on the walls are cancelled thanks to the material and geometry used. Other technologies can be used to characterise the interaction; hot-wire anemometers [39, 40], Pitot tubes [40] and Particle Image Velocimetry (PIV) [40–42] are used to describe the flow velocity. High velocity near cavities, struts, and other non-aerodynamic geometries produces noise. The aforementioned tools help visualise the flow and the eventual apparition of vortexes. Hot-wire anemometry relies on fragile wire probes that adapt their voltages to maintain constant temperature. A strong air flow will tend to cool down the wire, resulting in an increase in voltage to maintain the temperature. After a calibration, it is possible to use hot-wires to determine the flow velocity. In the same way, Pitot tubes measure the difference between static pressure and the stagnation pressure. The difference is called dynamic pressure, which can be traced back to flow velocity. Particle Image Velocimetry is based on capturing images of floating particles and calculating their movements between two frames. It gives a very easy-to-understand representation of the flow. Fig. 2.6 gives an example of the use of PIV to visualise the interaction of a planar jet in crossflow, during studies on the aircutain technology (see 2.1.5) [4].

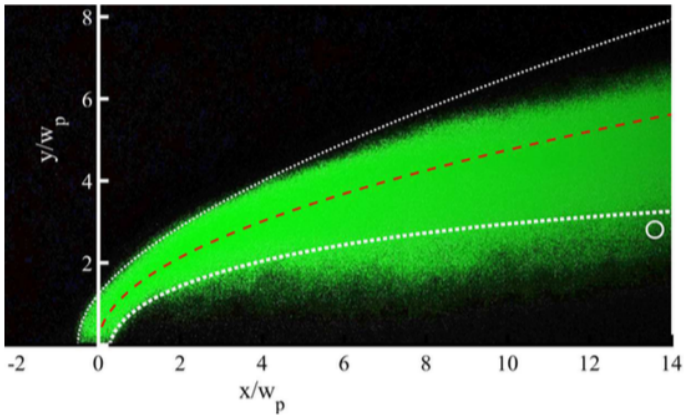

Figure 2.6: Flow visualisation of a single air curtain in a cross flow [4]

When looking at ways to predict noise coming from airplanes, the three approaches mentioned above are often used together, to verify the accuracy of the results. Measures of flow velocity can be coupled with microphone arrays' tests. All technologies aiming to reduce noise generation from the landing gear need to be thoroughly tested to ensure its efficiency and its impact on the landing gear's stability.

2.1.5 Review of noise reduction technologies

With the recent interest in reducing noise generated by landing gears, Low-Noise Technologies (LNTs) were developed during research programs. The main potential modifications are presented in the following paragraphs.

Solid fairings

Fairings are solid casings that act as shields to protect non-aerodynamic parts from high-velocity incoming flow. Such flow would generate undesirable noise going through bluff bodies. Fairings can be solid and protect elements like the axles or the wheel hubs. They can also be porous and take the form of meshes that slow down the incoming airflow.

Fairings have been widely used in research [2, 43, 44]. During the ALLEGRA (Advanced Low Noise Landing Gear for Regional Aircraft) project, different types of fairings were tested on a full-scale nose landing gear [43]. All the fairings had a medium to high TRL and included a ramp door spoiler, a solid wheel axle fairing, wheel hub caps and perforated fairings. Testing of multiple combinations were conducted using microphone arrays in a wind-tunnel environment. Results showed that the use of each fairing individually led to a lower noise level (- 6dB for the solid wheel axle fairing in the flyover direction). The study also underlined the complexity of combining fairings, sometimes leading to better noise reduction but also resulting in higher noise level when the air flow deflected by a first fairing went through other unshielded geometries. The fairings' impact on noise reduction can be different, depending on the evaluated frequencies and the direction of the noise, either in flyover or side direction. Some fairings have been flight-tested [32], comparing a baseline performance with other flyover situations where fairings where fixed on the landing gears. Fig. 2.7 shows the use of fairings on a Boeing main landing gear. The noise levels measured during the flyover tests confirmed the results from the empirical model: the use of solid fairings helped with reducing noise coming from the landing gears.

Potential for noise reduction set aside, the presence of fairings can also have an impact on brake cooling, with the reduction of incoming air through the landing gear. As mentioned before, volume and weight are important constraints when designing new technologies for landing gear, as well as leaving the opportunity for a visual inspection. For these reasons, only wheel hub caps have been implemented so far.

Figure 2.7: "Toboggan"-like fairing attached to the B777-300ER main landing gear in the QTD 2 Project [3]

Porous fairings and meshes

Porous fairings and meshes are other Low-Noise Technologies. The difference with previously mentioned technologies is that porous materials allow a partial air circulation and therefore should reduce the deflected flow which can hit other non-aerodynamic geometries. In this study [43], a perforated fairing is used to protect several regions of the landing gear (lower arm, steering pinion and wheel axle). The study points out the main parameters for designing a perforated fairing or a mesh: the diameter of the holes and the porosity of the material. The difficult tuning of both parameters is summarised in [18]. While too high porosity would mean too much flow reaching the protected areas and possibly generating noise, little porosity would increase the weight and have an outcome similar to solid fairings. The diameter of the holes is also very important, as they can generate high-frequency noise is not properly designed. A possibility would be to reduce the diameter and aim for frequencies higher than the audible range. Ongoing studies explore the impact of perforated fairings on reducing flow velocity, vortexes and noise [45]. Although some advantages like lower flow velocity and less low frequency noise are observed, other disadvantages appear: high frequency noise and shear-layer noise.

Because security is the main priority in aviation, the implementation of porous materials is complicated, as they would be placed around existing structures. Studies on their impact on the structure's functionality would need to be conducted.

Air curtains

Air curtain is the Low Noise Technology studied in the following chapters. It can also be referred to as planar jet. The objective with the air curtain is to protect the landing gear by

creating an air shied around either the whole landing gear or the targeted regions. Air coming out of jets at high velocity would interact with the ambient air flow and create a protective layer around the landing gear, reducing the flow-induced noise. The original patent was released in 2004 by Sijpkes and Wickerhoff [5], see Fig. 2.8.

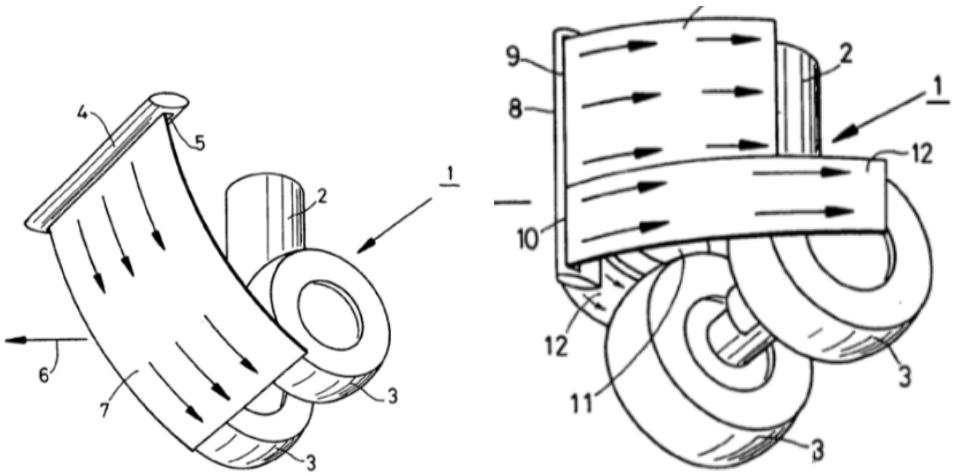

(a) Single air curtain (b) Dual air curtain

Figure 2.8: Examples of the air curtain layout for landing gear noise reduction [5]

Different configurations have been tested, using single-jet or dual-jet air curtains to shield various bluff bodies from a high-velocity cross-flow. First study confirmed the potential noise reduction properties of air curtains [46]. A configuration yielded encouraging results, with a noise level reduction of 3 to 5 dB. This first study also outlined the correlation between the blowing slot noise and the 5^{th} power of the jet speed, warning that the jet slot could become the main source of noise at certain frequencies and velocities. Following this first proof of concept, studies of one or two air curtains shielding bluff bodies have been conducted [4, 19, 42]. Zhao et al. [19] first tested how a single-jet air curtain could help reduce the noise generated by tandem rods. PIV and aerodynamic tests using hot-wires helped conclude that the air curtain limited the air velocity around the tandem rods. Reducing the flow velocity also helped limiting vortex shedding and interactions of said vortexes, created by the first rod, with the rear rod. However, at some frequencies, the noise contribution from the planar jet is superior to this of the rods. The following studies [4, 42] focused on dual planar jets, using empirical, numerical and experimental methods. The objective was to characterise the interaction between two parallel planar jets and observe potential new vortexes. The combined use of air curtains implies two recirculation zones between the jets, with different flow velocities, and turbulence when the two jets come together. Using CFD to find the

optimal position for a bluff body (tandem rods), a single jet was compared to dual jets. The single jet once again could be the main noise source at certain frequencies. Dual jets really proved valuable because they can achieve the same shielding height with a lower jet velocity, therefore reducing the jets' contribution to noise generation.

Aforementioned studies confirm that the air curtain technology could be useful for shielding non-aerodynamic component of landing gears. Such technology is highly attractive, as it is not as invasive and heavy as fairings, and would allow visual inspections necessary for maintenance.

Research on this technology is still in its early stages, with tests conducted on bluff bodies and air curtain' geometries to be determined. This present report now aims to explore the integration of air curtain on scaled-down replicas of landing gears in wind tunnel situations, and the potential impacts in terms of noise reduction and flow velocity.

2.2 Summary

Research has proven that the landing gear was responsible for a significant proportion of the airframe noise during aircrafts' takeoffs and landings. As a result, Low-Noise Technologies have been developed using empirical, numerical and experimental noise prediction methods. Low-Noise Technologies range from solid fairings to meshes and air curtains. The use of air curtains has yielded encouraging results: it has helped reducing the flow velocity around rods and the noise level at certain frequencies. This report aims to use air curtains on realistic scaled-down landing gears and study their impact on noise levels.

Chapter 3

Methodology

The research objective is to study the use of air curtains on scaled-down landing gears. In this chapter, procedures for test, both experimental and numerical, are presented. The experimental section describes the rig for hot-wire anemometry tests, as well as the steps to follow. It also includes a description of sound-level tests. The numerical section describes the software and parameters used for the numerical analyses.

3.1 Experimental method

The physical tests conducted during the project covered two points: the air velocity coming out of the air curtain, and the associated noise level. Knowing the air velocity is a key requirement, as it is linked to the shielding height and the capacity to protect downstream geometries. It's also linked to noise generation, as low-velocity zones inside the air curtain can be responsible for recirculation noise. The sound-level tests are necessary to control that air curtains do not become new noise sources. This section focuses first on flow-velocity tests using hot-wire anemometry.

3.1.1 Working principle of hot-wire anemometry

Hot-wire anemometry is the use of a hot wire to measure the air flow velocity at a known point in space. A fragile probe with a thin wire is positioned in the air flow. It is connected to a data acquisition system. The wire is heated up to 80% of its maximal temperature by modifying the voltage. The acquisition system then adjusts the voltage in real time to keep the wire's temperature constant while the air flow cools it. The changing voltage is therefore directly linked to the air flow velocity. With calibration, it is possible to measure the voltage at discreet points and to calculate the corresponding flow velocity.

As mentioned in the literature review, there is a correlation between the blowing slot noise and the 5^{th} power of the air speed. This test monitors the flow velocity coming out of the air curtains. It's also used to plot the velocity profile and to monitor how homogeneous the flow is.

3.1.2 Calibration for flow-velocity tests

Description of calibration set-up

The rig used for hot-wire calibration is presented in Fig. 3.1. It is made of 5 main elements. All additional pictures can be found in Annex A.

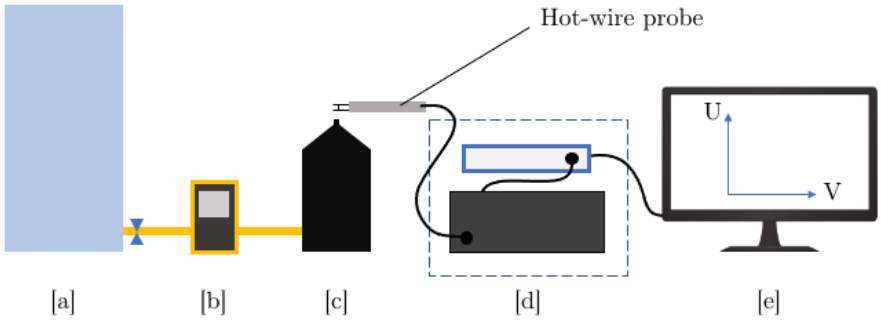

Figure 3.1: Test rig schematic for calibration with [a] the compressed-air tank, [b] the flow-rate meter, [c] the chamber, [d] the Data Acquisition System, and [e] StreamWare Pro software

First, a tank [a] is filled with compressed air. It gives the advantage of storing the compressed air close to the rig and allows a steadier and more reliable air supply. The cylinder valve controls the air flow coming into the calibration system.

A flow-rate meter [b] then displays the air flow rate through the system in Standard Litre Per Minute (SLPM).

The air then goes in a chamber [c] designed to redirect the flow upwards in a clean column. The hot-wire probe is place directly above the chamber's opening.

The hot-wire is connected to a Data Acquisition System (DAS) [d] made of two modules: a StreamLine 90N10 Frame with a Constant Temperature Anemometry (CTA) system by Dantec Dynamics and a PXI-1033 controller by National Instrument. The DAS allows for the Frame to control the hot-wire's temperature and sends to the computer the corresponding voltage as well as the ambient temperature, taken into account to correct the measured values.

A computer [e] runs Dantec Dynamics' StreamWare Pro software. The DAS is recreated in the software, using the specifications of the cables and the probe (type, length, resistance). Adjusting the gain and the offset gives more precise values. The offset changes the voltage for the neutral value (no flow), while the gain multiplies the voltage measured by a given number. This way, the measurements can vary between 1 and 8V, rather than 2.5 and 3.5V. The window is more adapted, making variations more visible.

Steps for calibration

The objective of the calibration is to find the correlation between a measured voltage and flow velocity. For an accurate correlation, it is required to make enough measurements on

a broad range of velocities. The calibration for this project used 15 points evenly spaced between 26 SLPM and 390 SPLM, maximum rate of the flow rate meter.

The first step is to modify the flow rate coming out of the air tank by turning the cylinder valve and reach one of the 15 targeted flow rates. The second step is to turn the flow rate value Q into a flow velocity value V_{flow} . Because the section area of the chamber outlet $A_{section}$ is known, it is possible to calculate the flow velocity using Equation 3.1:

$$V_{flow} = \frac{Q * 0.001}{A_{section} * 60} \tag{3.1}$$

Once the velocity is calculated, it can be typed into the calibration tab of StreamWare and the corresponding voltage is read. A table of voltages U and velocities V_{flow} can be saved and used either in Excel or Matlab to do a polynomial interpolation. For this project's calibration, the interpolation was the following, see Equation 3.2:

$$V_{flow} = 0.153U^4 - 2.2777U^3 + 15.114U^2 - 42.997U + 45.308 \tag{3.2}$$

3.1.3 Flow-velocity tests

Description of flow-velocity-test set-up

For flow-velocity tests on air curtains, the flow-rate meter is removed and the air curtain is placed after the chamber [b] in Fig. 3.1. The modified schematic is shown in Fig. 3.2.

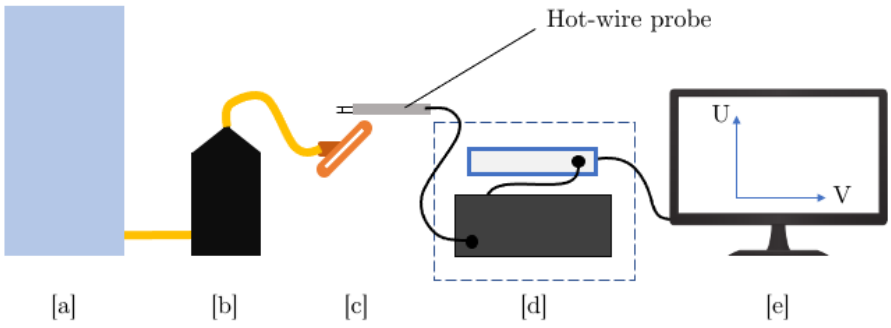

Figure 3.2: Test rig schematic with [a] the compressed-air tank, [b] the chamber, [c] the air curtain, [d] the Data Acquisition System, and [e] Matlab

The probe is held by a traverse with Computer Numerical Control (CNC), controlled via Arduino boards and Matlab code. All axis are equipped with stepper motors and can be operated 2 at a time (X-Y, X-Z or Y-Z), moving the probe along a single plane during a test.

Steps for flow-velocity tests

The first step is to identify what path should the probe follow, where should it stop for measurement, and to fill the Matlab code accordingly: number of values span-wise/stream-wise, and corresponding number of motor steps between two points.

Once the probe path is settled and the compressed air supply connected to the air curtain, the Matlab code can be run to acquire data. Voltage is acquired at each point of the path with a rate of 1000 scans per second, for 5 seconds. For each point, voltages are averaged and the resulting voltage is translated into a flow velocity using Equation 3.2. The flow velocity is stored in a "results" variable. The results need to be saved immediately after the test.

The last step is to use another Matlab code with the "results" file, in order to plot a velocity contour. "Data acquisition" Matlab code and "visualisation" code are available in Annex B.

3.1.4 Sound-level tests

To compare noise coming from the air curtains, sound-level tests are necessary. Without access to an acoustic calibrator, absolute results should be interpreted carefully.

A Sound-Level Meter (SLM) is placed on a tripod at 3 different locations. Additional pictures are shown in Appendix C. The model used during this research project is the SVAN 971 by Svantek. The measurement locations are marked on the ground to ensure test repeatability. They are represented in Fig. 3.3. Position [a] will be later referred to as "Near left", position [b] "Far left" and position [c] "Far behind". The value taken is a measurement of the equivalent continuous sound level, written Z_eq on the screen. It gives the constant noise level equivalent to the total energy produced over a time period by a fluctuating noise. Each measurement lasts for 30 seconds to ensure the capture of a representative time period. Two values are taken at each location, one "ambient" value, without flow coming out of the air curtain, and one "test" value, with the air curtain blowing air and producing noise. These two values allow a relative measurement of the noise generated by the air curtain, by subtracting the ambient noise level to the test noise level.

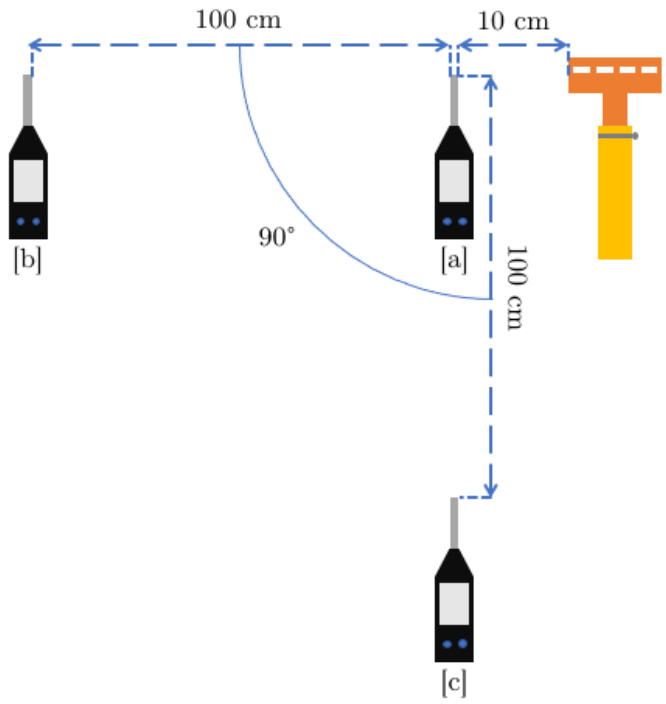

Figure 3.3: Locations of SLM during sound-level tests

3.2 Numerical method

The numerical tests were conducted using Ansys Fluent to recreate the air flowing inside and outside the air curtain, both in crossflow and in quiescent conditions. The objective was both to predict how the flow would interact with the geometry and to modify the geometry before printing, and to check that the experimental results stay consistent in similar numerical conditions. The following sections comment on the steps followed to achieve 2D and 3D analysis, as well as the parameters used.

3.2.1 Geometry definition

The first step of a numerical test is to define the geometry to be tested. For 2D tests, the plane of interest is selected. Within the SolidWorks part file, the corresponding plane is isolated, with sketch lines drawn at the intersection of the part and the plane. A rectangle is sketched around the air curtain to represent the ambient flow. The sketch is then converted in a planar surface, where the air curtain is represented as a hole in the surface, see Fig. 3.4(a). The planar surface is saved as a ".sat" file. For 3D tests, the part is subtracted to

a box representing the ambient flow, creating a hole in the fluid with the shape of the air curtain, see Fig. 3.4(b). The resulting box is also saved as a ".sat" file.

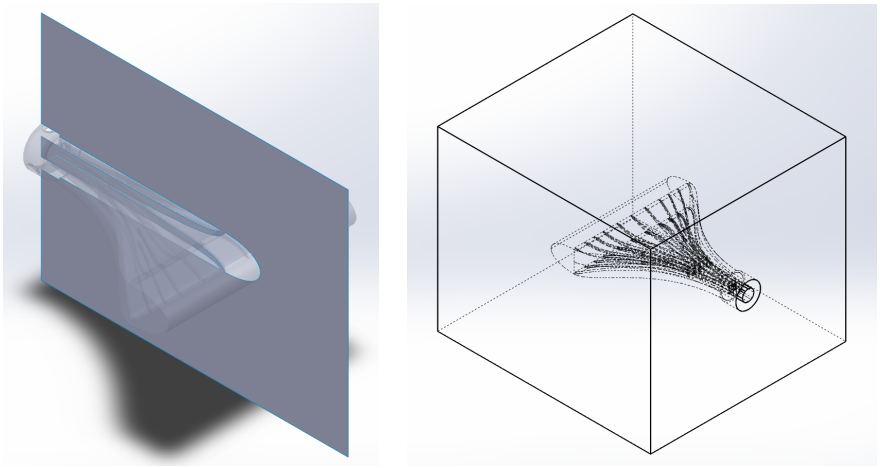

(a) 2D geometry extraction (b) 3D geometry extraction

Figure 3.4: Geometry extraction of 2D and 3D files for Ansys Fluent analysis

3.2.2 Geometry preparation and mesh

The next step is to upload the geometry to the Ansys Fluent project and to name selected geometries in order to facilitate the future set-up of the tests. In DesignModeler, the body type is changed to fluid. Faces or edges are selected in turn and named according to their boundary conditions. There are 4 different boundary conditions and 4 corresponding named selections, shown in Fig. 3.5:

- "wall": all the faces/edges representing the air curtain can be renamed "wall" because they will have a "wall" boundary condition (stationary, no slip, standard roughness), see Fig. 3.5(a);
- "jetflow": the flow coming in the air curtain comes out of a surface/edge called "jetflow", with a variable inlet velocity boundary condition, see Fig. 3.5(b);
- "crossflow": the ambient flow recreating the speed of the aircraft through the air comes out of a surface/edge called "crossflow", with a variable inlet velocity boundary condition, see Fig. 3.5(c);
- "freeflow": the ambient flow around the air curtain is supposed to be infinite, which is why there are surfaces/edges called "freeflow" with an pressure outlet boundary condition, see Fig. 3.5(d).

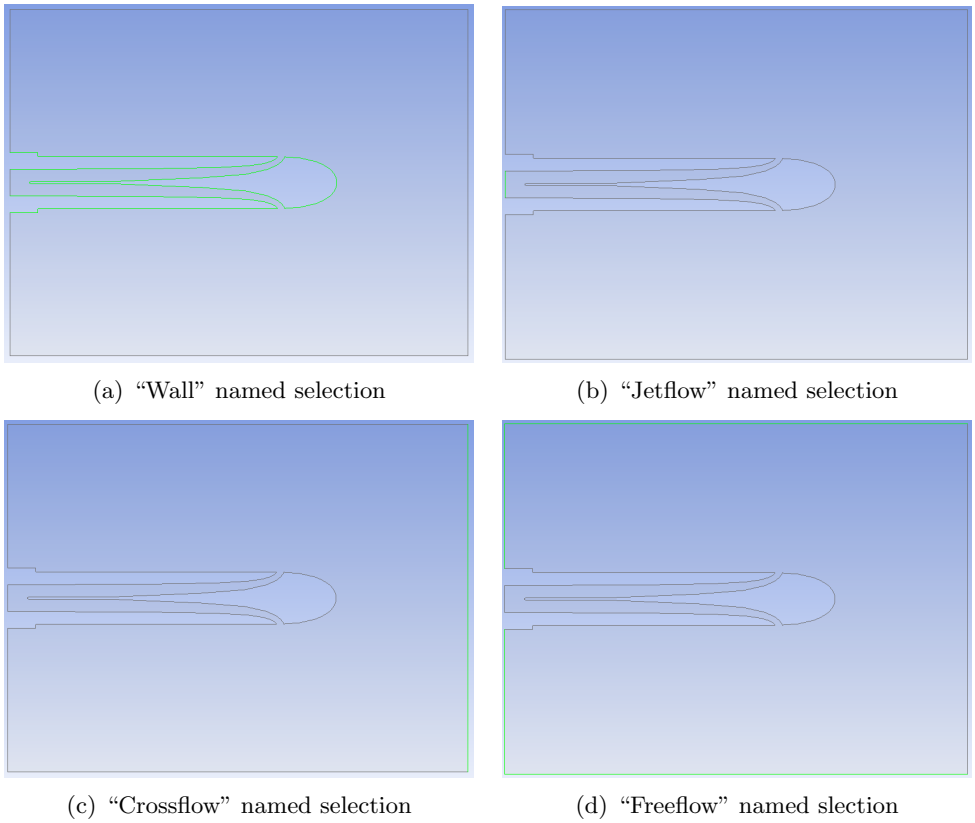

(a) "Wall" named selection (b) "Jetflow" named selection

(c) "Crossflow" named selection (d) "Freeflow" named slection

Figure 3.5: The four named selections for the corresponding four boundary conditions on a 2D geometry

It can also be helpful to name at this time the centres of future spheres of influence, which allow for a finer mesh at important locations, see Fig. 3.6(a).

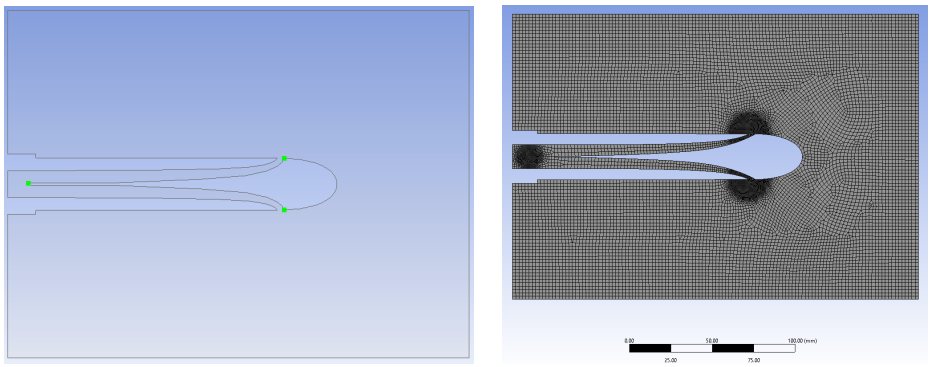

(a) Location of centres (b) Resulting mesh

Figure 3.6: Example of a 2D mesh (2mm elements) using spheres of influence (7mm/12mm radius, 0.5mm elements)

Next, a mesh needs to be applied to the geometry. In these tests, the average mesh varied from 2 to 3mm, and spheres of influence were used to create a finer mesh where the fluid/solid

interactions should be more complex (baffles start and air curtain outlets). Mesh within these spheres went down to 0.2mm. An example is shown in Fig. 3.6.

3.2.3 Boundary conditions and calculation

Once the mesh is generated, boundary conditions are applied to the corresponding named selections, as described previously. The CFD model used is Transition SST (4 equations). When all the conditions are correctly stated, the analysis is initialised and calculated. The final step is to generate velocity contours along the desired surfaces/planes.

Chapter 4

Preliminary results

This project was divided in two parts; a preliminary part focused on testing a wide range of curtains ahead of a test campaign in Germany, followed by iterative redesign, using experimental and numerical results.

The preliminary part was centred on air curtain geometries to be mounted on two landing-gear models. The global objective of this phase was to test the models in Germany, in an anechoic chamber, with different air curtains. Before testing the air curtains in DLR's wind tunnel, the goal was to characterise the flow of a wide range of air curtains at TCD, in a quiescent conditions.

This chapter describes the first air curtain designs, as well as the results of TCD tests, both using hot-wire anemometry and CFD. The results from Germany are also presented. Lastly, all results are discussed and potential improvements are outlined.

4.1 Air curtain geometries

Twenty-two air curtains, with different geometries, were tested during this 1^{st} part. They are divided in two categories: air curtains mounted directly on the landing gear, and air curtains located upstream. Their main geometric features are described and listed in Tables 4.1 and 4.2.

The shorter air curtains are designed to shield the wheel axle. Seven are designed for the smaller model, three for the larger one. They vary in slit width and wall thickness, as described in Table 4.1.

Longer air curtains are designed to be located in front of the wheels and the wheel axle to shield them from the ambient cross-flow. Geometries are described in Table 4.1.

Asymmetrical air curtains are designed to shield the torque link situated above the wheels. They are described in Table 4.1.

The last air curtain geometry tested is the strut geometry, located in front of the landing gear and fixed to the fuselage. Its objective is to shield the entire landing gear. A different geometry parameter was tested at this point, with a change in the slit width and wall thickness at the middle of the air curtain. The geometry descriptions are given in Table 4.2.

The different locations of air curtains can be seen in Fig. 4.1 and Fig. 4.2.

Table 4.1: Description of on-landing-gear air curtains

Landing gear		Location	Slit width (mm)	Wall thickness (mm)
SLG	LLG			
√		Wheel short	1	*
√		Wheel short	1	*
√		Wheel short	1	*
√		Wheel short	2 or 3	2 or 3
√		Wheel short	2 or 3	2 or 3
√		Wheel short	2 or 3	3 or 4
√		Wheel short	2 or 3	3 or 4
√		Wheel long	1 or 2	2
√		Wheel long	1 or 2	2
√		Wheel long	2 or 3	3 or 4
√		Torque link	1 or 2	2
√		Torque link	2 or 3	3 or 4
	√	Wheel short	1 or 2	3 or 4
	√	Wheel short	3 or 4	3 or 4
	√	Wheel short	3 or 4	5 or 6
	√	Wheel long	4	6
	√	Wheel long	4	3
	√	Torque link	2	3

* Slit width too small to allow measurement

Table 4.2: Description of upstream air curtains

Location	1st slit width (mm)	1st wall thickness (mm)	2nd slit width (mm)	2nd wall thickness (mm)
Upstream	2	9	3 or 4	6
Upstream	2	6	4	9
Upstream	4	6	2	9
Upstream	2	7 or 8	*	*

* No change in slit width or wall thickness

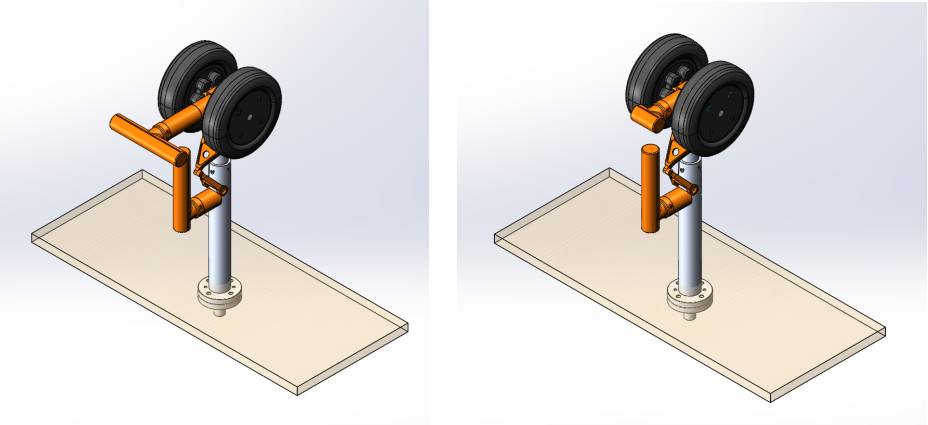

(a) Larger landing-gear model with a long wheel air curtain, and a torque-link air curtain

(b) Larger landing-gear model with a short wheel air curtain, and a torque-link air curtain

Figure 4.1: Two assembly configurations for the larger landing-gear model

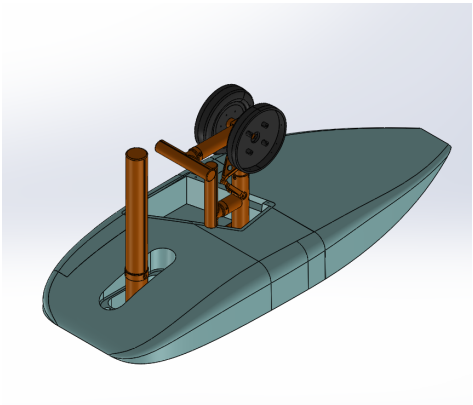

Figure 4.2: One of the assembly configuration for the smaller landing-gear model, with an upstream strut, a long-wheel air curtain, and a torque-link air curtain

4.2 Results

4.2.1 Flow-velocity tests

In this subsection, only the results for the wheel air curtains (short and long) are shown, because the rest of the project is focused on this type of geometries. Examples of results for the other geometries can be found in Annex E. The results commented in this subsection are listed below:

- Two short wheel air curtains designed for the larger landing gear with different wall thickness and same slit width (Fig. 4.3);
- Two short wheel air curtains designed for the larger landing gear with different slit width and same wall thickness (Fig. 4.4);
- A long wheel air curtain designed for the smaller landing gear (Fig. 4.5).

In Fig. 4.3, velocity profiles from similar air curtain geometries with different wall thicknesses are shown. Both profiles display a high velocity peak at the centre, aligned with the flow inlet, and two smaller velocity peaks at each extremity of the slit. The velocity magnitudes are also very similar.

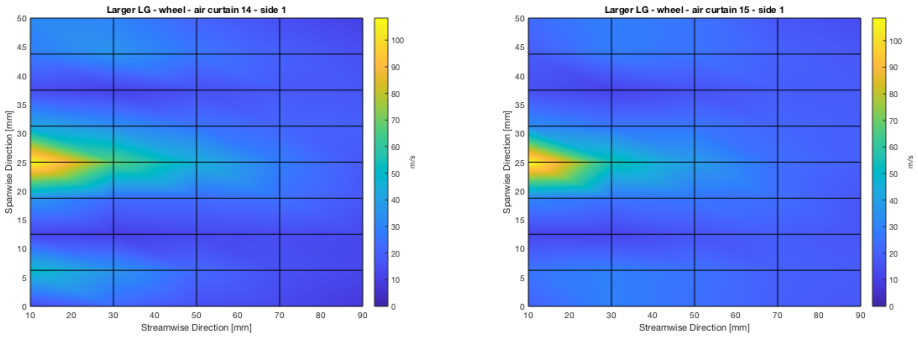

(a) Wall thickness 5mm (b) Wall thickness 3mm

Figure 4.3: Velocity profiles of similar short wheel air curtains with different wall thickness, using HWA

In Fig. 4.4, air curtains with same wall thickness/different slit width are compared. There is a small difference in the highest velocity reached: 108.7 m/s for the 4mm-slit-width air curtain, and 116.0 m/s for the 1.5mm slit-width air curtain. The flow distribution is also different, with a larger central peak on Fig. 4.4(a), and higher peaks on the extremities as well.

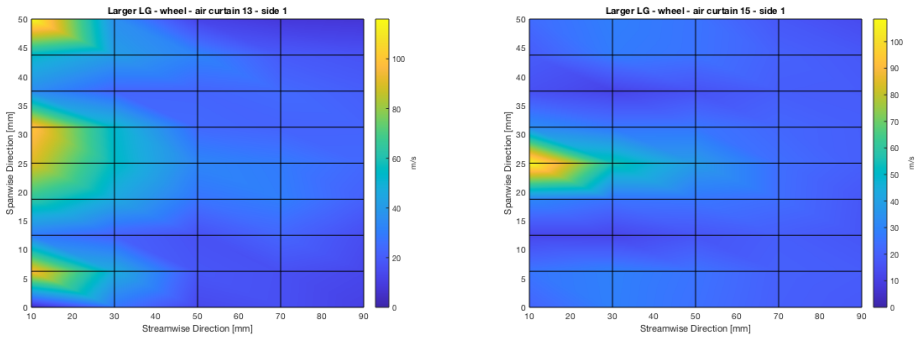

(a) Slit width 1.5mm (b) Slit width 4mm

Figure 4.4: Velocity profiles of similar short wheel air curtains with different slit width, using HWA

Finally, in Fig. 4.5, velocity profiles of both sides of an long wheel air curtain are plotted. Results are different from the short wheel air curtains in two ways; the air velocity coming out of the long wheel air curtain is generally lower, and the flow distribution is different, with stronger flow at the extremities.

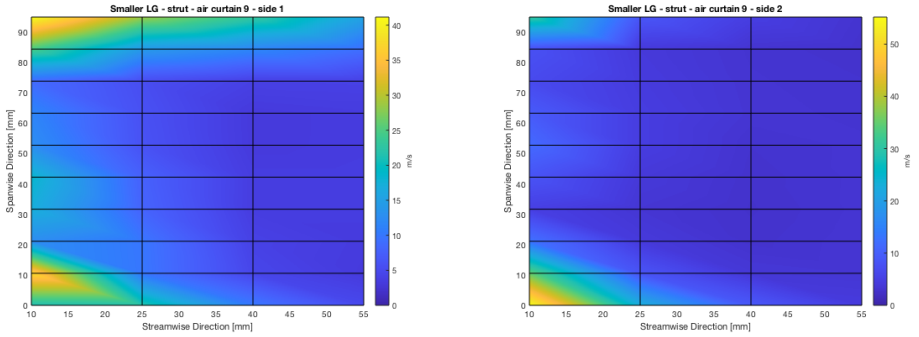

(a) Side 1 (b) Side 2

Figure 4.5: Velocity profiles of a long wheel air curtain, using HWA

4.2.2 Sound-level tests

Acoustic tests were performed in Germany [47]. The model landing gear was placed in an Aeroacoustic Wind Tunnel and tested in different conditions: quiescent environment (wind tunnel off) and no jet flow from the air curtain, jet flow activated but quiescent environment and jet flow combined with cross-flow. The objective of these tests was to detect the geometry responsible for the noise and measure that noise level. The set-up is shown in Fig. 4.6. The results are shown in Fig. 4.7. It should be noted that, although it is represented, the torque-link air curtain was not present during the test.

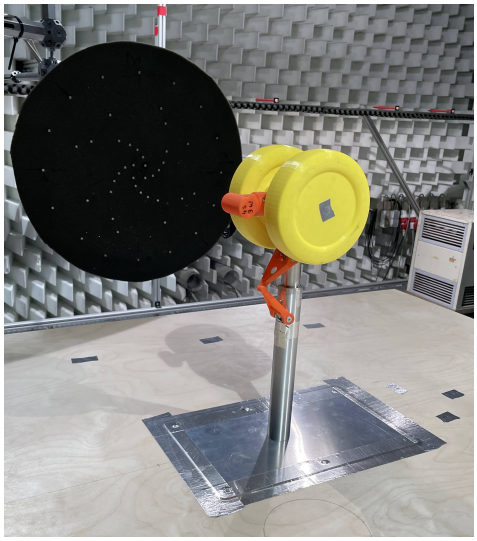

Figure 4.6: Model landing gear (short wheel air curtain configuration) placed in the wind tunnel with a microphone array behind

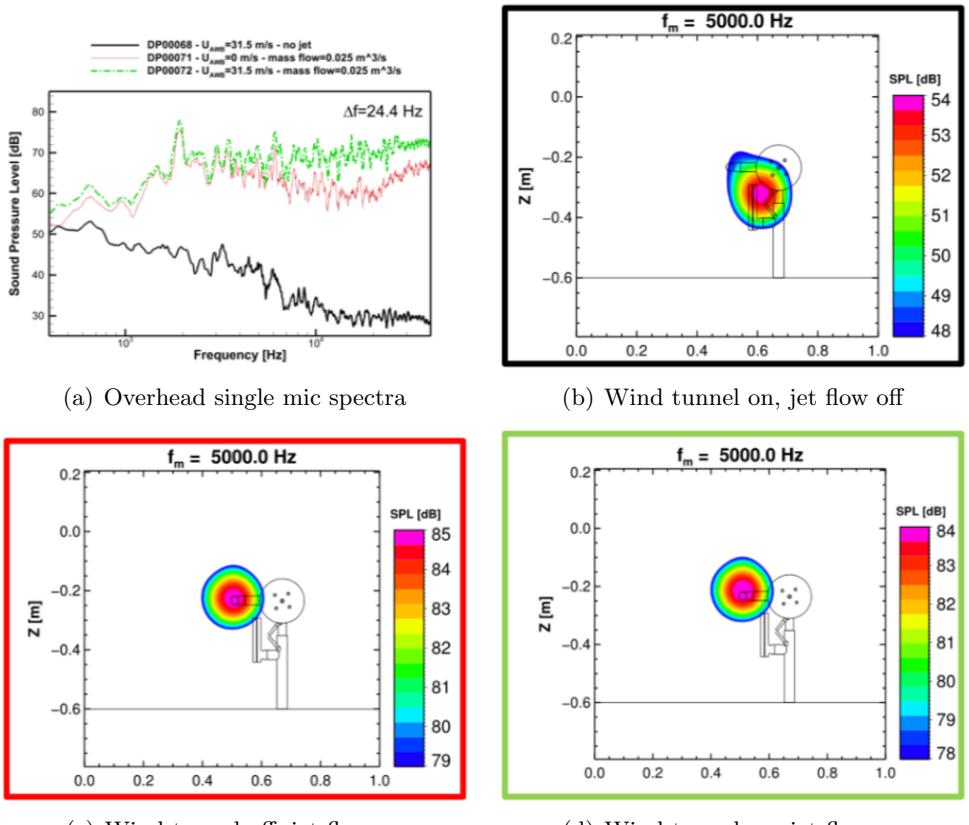

(a) Overhead single mic spectra

(b) Wind tunnel on, jet flow off

(c) Wind tunnel off, jet flow on

(d) Wind tunnel on, jet flow on

Figure 4.7: Spectra and beamforming results: larger model landing gear, short wheel air curtain with jet flow velocity of 31.5 m/s

These first tests show that the air curtain itself is a great source for noise. The noise levels are significantly higher as soon as the jet flow is introduced. This is reinforced by the

results of the beamforming at 5000 Hz, which point the torque link and the air curtain as noises sources, with the torque link causing noise going up to 54 dB. In the two other tests (see Fig. 4.7(c) and 4.7(d)), the jet flow coming out of the air curtain is the main source of noise, with noise levels going up to 85 and 84 dB.

Another test was conducted, where a small diameter rod was added to the torque link, in order to generate a whistling sound when placed in a cross-flow. The whistling sound can be seen in Fig. 4.9(a), with a peak at 4000 Hz. The air curtain used this time was a modified version of the torque-link air curtain, see Fig. 4.8. The beamforming done at 4000 Hz confirms that the whistling sound comes from the rod on the torque link, with a noise level of 72 dB. This time, once the jet flow is activated, the air curtain reduces the sound level to 60 dB, suppressing the noise of the cross-flow touching the rod.

Figure 4.8: Modified torque-link air curtain with added rod for whistling sound

4.2.3 CFD analysis

In order to understand what could be the reason of such noise, a CFD analysis was conducted. CFD analysis was used to predict the flow interaction with the air curtain, both inside and outside the geometry.

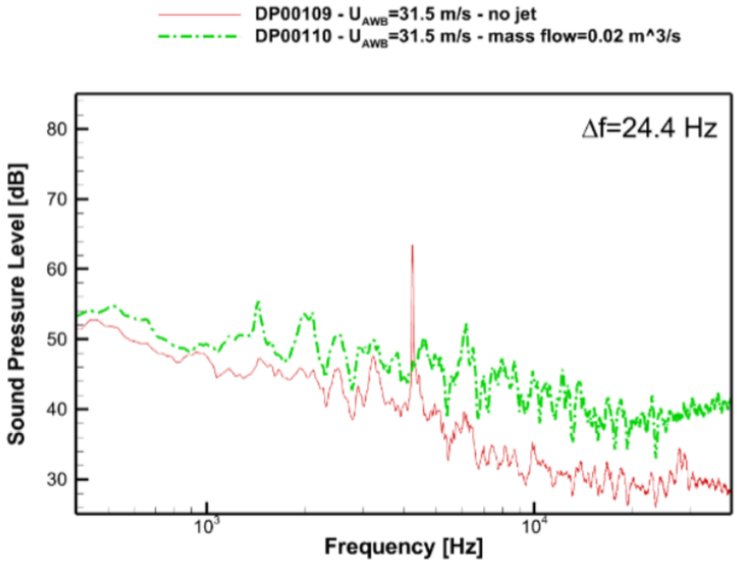

(a) Overhead spectra

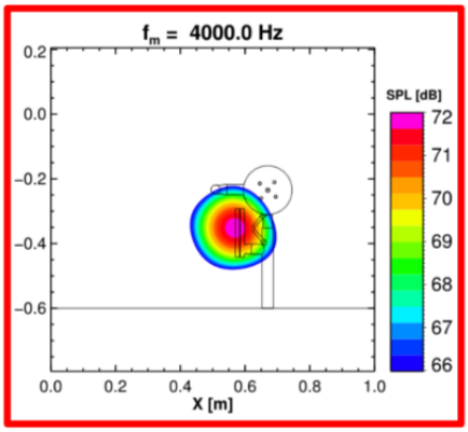

(b) Wind tunnel on, jet flow on

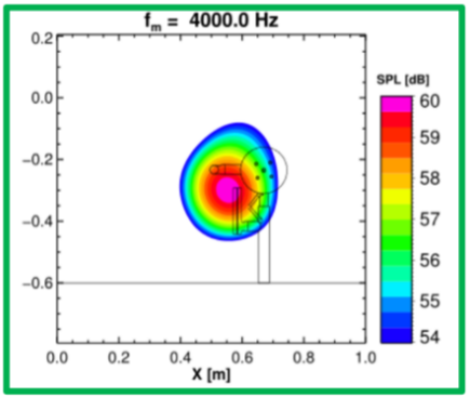

(c) Wind tunnel on, jet flow on

Figure 4.9: Spectra and beamforming results: larger model landing gear, modified torque-link air curtain with jet flow velocity of 31.5 m/s

A 2D analysis of a short wheel air curtain in a 65m/s cross-flow and a 65m/s inlet flow was done. The velocity contour is represented in Fig. 4.10. There are two main things to notice:

- The air curtain generally has the expected behaviour: it blows air at high velocity (red zones), which shields the air downstream (large blue zones), moving at a near-zero velocity.
- The blue zone inside the air curtain seems to indicate some recirculations at low velocity in the chamber.

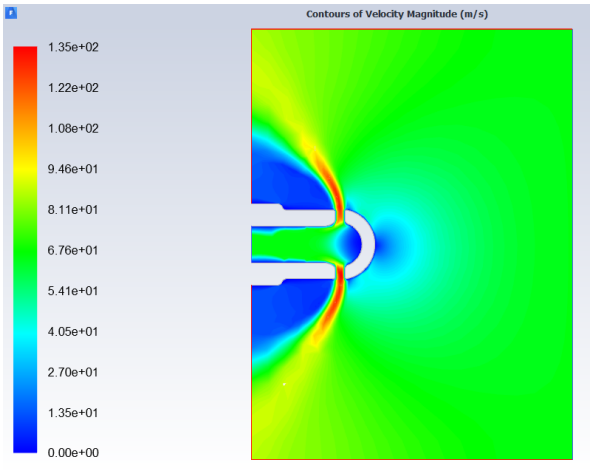

Figure 4.10: Velocity profile of a baseline air curtain, in a cross-flow, using Ansys Fluent

4.3 Discussion

The results of the CFD analysis, the hot-wire tests and noise level tests gave a first understanding of the air curtain flow mechanism. Although the "shield" action was present, there are a number of things that needs to be changed to reach a low-noise solution.

Focusing on the wheel air curtains, the flow heterogeneity needs to be addressed to achieve an evenly-spread shielding effect. Variations in design seems to have a varying impact on flow homogeneity. The wall thickness has little to no impact on the flow, while the slit width does have an impact on the velocity and the distribution. Knowing this, the next design could play with the slit width to achieve better results.

The air curtain location (wheel, torque link, upstream) means a different air inlet and changing constraints. For the remainder of this research project, the study focuses on wheel air curtains, with symmetrical geometries and a central air inlet.

The most important issue with these preliminary designs was the noise level, as illustrated by the tests in Germany. The air curtain was, most of the time, a significant noise source, adding to the noise generated by the landing gear in a cross flow. The final test with the reduced whistling noise is the exception that reaffirms the potential of air curtains as low-noise technologies.

An explanation for the high noise level could be the recirculation zones within the air curtain, as pointed out by the 2D CFD analysis. A future design should take this problem into account and look at reducing or getting rid of the "chamber" geometry. It can also be

concluded that the outside geometry is not optimal and could be enhanced to become more aerodynamic.

Finally, it is important to note that there are limits to the calibration process for flow-velocity tests: the flow meter cannot measure the highest flow rate the tank can provide, leading to a range of velocities during calibration smaller than the range of velocities during tests. This is not the ideal configuration because the measurements rely on the quality of the interpolation between voltage and calibration velocities. As a result, the velocity magnitudes measured during experimental tests should not be considered as absolutes. However, all measurements were taken using the same interpolation, which guarantees a proportionality between the results.

Chapter 5

Results

Following the preliminary tests, the project was centred on enhancing the performance of wheel air curtains; both in terms of noise and of flow distribution. Two new designs were developed successively, and compared to the baseline (see Fig. 5.1(a)). This chapter is therefore divided in two parts, corresponding to each design.

5.1 Short wheel air curtain with baffles

Taking in the findings from the preliminary tests, the design of the short wheel air curtain was changed. In this section, the new geometry is described, as well as the results of both hot-wire-anemometry tests and CFD analysis. Results are discussed and new guidelines are established for the next design.

5.1.1 Air curtain geometry

Several changes were made to the baseline design (short wheel air curtain), in answer to its previous performances, both at TCD and in Germany, in DLR's wind tunnel. They can be divided in 3 main changes:

- The chamber has been removed. The recirculation within the cylindrical chamber could have been a source of noise in the baseline design. This new geometry aims to bring the inlet flow straight out following a clear path and avoid recirculation.
- Baffles have been implemented. In order to counter the uneven flow distribution along the air curtain's slit, baffles are used to divide the inlet flow and to force the air to come out at regular intervals. There are 3 baffles, dividing the air curtain slit in four equally-sized rectangular openings.
- The outside geometry has been modified to be more aerodynamic. Because the air curtain placed in a cross-flow was already a source of noise during DLR's tests, the outside shape has been modified to be less "bulky".

The baseline design and the new design are presented in Fig. 5.1.

5.1.2 Results

Flow-velocity tests

The objective at this point was, once again, to characterise the flow coming out of the air curtain and check the noise level. By feeling the flow once the short wheel air curtain with

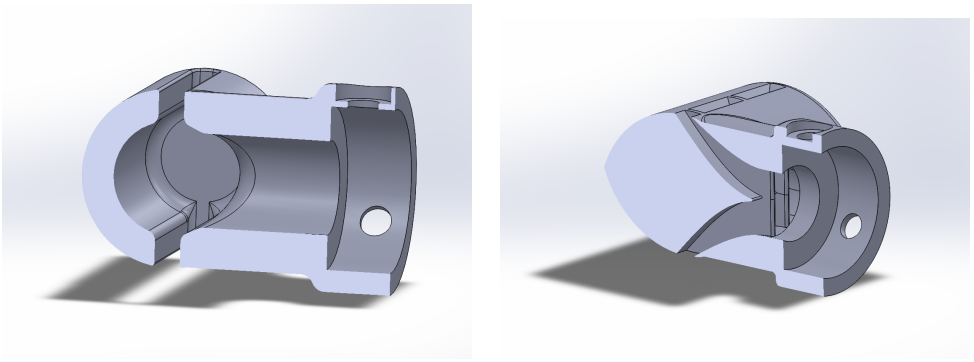

(a) Baseline design (b) New design

Figure 5.1: Comparison of section views: baseline design from the preliminary tests, and new design for the short wheel air curtain

baffles was set up on the TCD rig, 4 study planes were selected. The vertical plane is represented in Fig. 5.2. The 3 remaining planes are shown in Fig. 5.3.

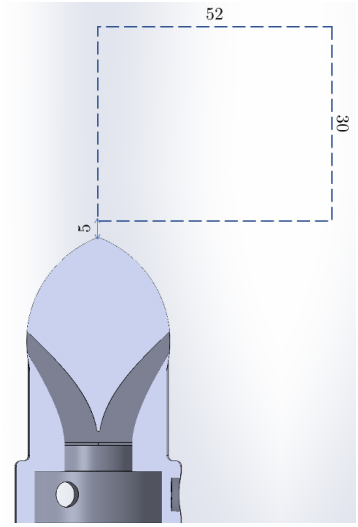

Figure 5.2: Location of study plane - vertical plane

The corresponding velocity contours are shown in Fig. 5.4. These contours were obtained in quiescent conditions (wind tunnel off). All contours put together show that the direction of the out-coming flow is different from the previous design, where the air is coming out at a 90° angle. With this design, the air is coming out at a smaller angle. From this first multi-plane study recreating a 3D visualisation, the main observations are:

- The peak velocities is higher the closer you are to the air curtain. In Fig. 5.4(b), the peak flow velocity is around 115 m/s, 10mm away from the air curtain, while it is only 62 m/s 10mm further away in Fig. 5.4(d). In Fig. 5.4(a), the flow velocity rapidly

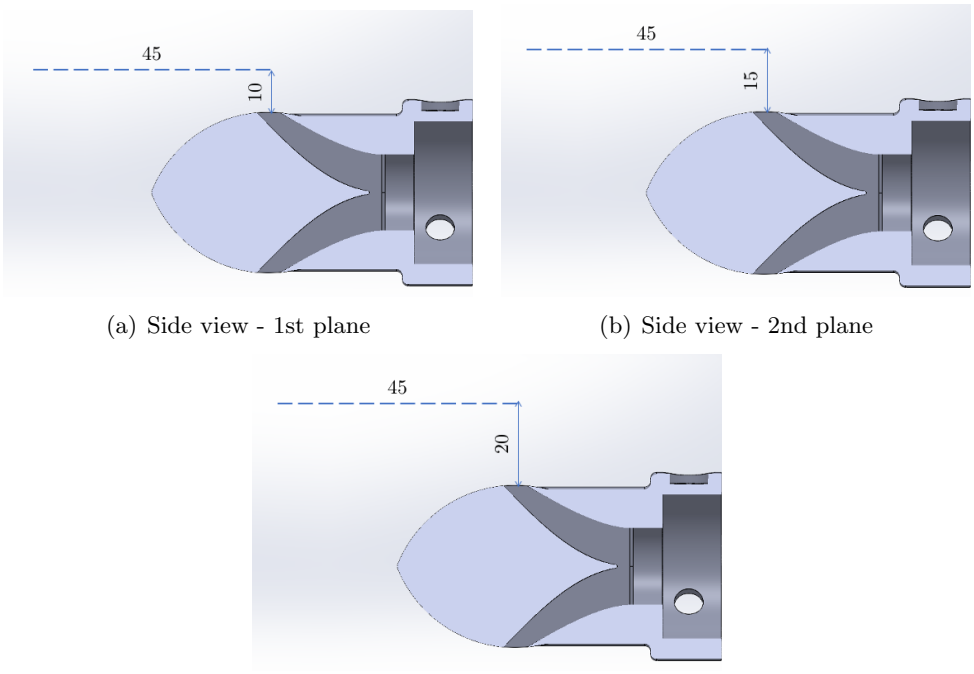

(a) Side view - 1st plane

(b) Side view - 2nd plane

(c) Side view - 3rd plane

Figure 5.3: Location of study planes - horizontal planes

decreases from 62 m/s to around 35 m/s with an increased distance to the air curtain (15 mm difference).

- These peak velocities are more concentrated the closer you are to the air curtain. In Fig. 5.4(b), the high velocities form a narrower crescent than in Fig. 5.4(d), where the high velocities are more spread out.

- The flow distribution is still heterogeneous. The highest velocities is still concentrated at the middle of the air curtain. In the mean time, the resulting crescent of air, coming out of the air curtain, has a velocity of minimum 27m/s at its left extremity, for the farthest plane, see Fig. 5.4(d).

During the hot-wire tests, the air curtain was still very loud and required the use of ear protections.

CFD analysis

The first objective of the CFD analysis was to compare the new design to the previous one. A 2D analysis was then conducted to check how the flow interacts with a "no-chamber" design. The results are presented in Fig. 5.5. Both simulations were run with the same boundary

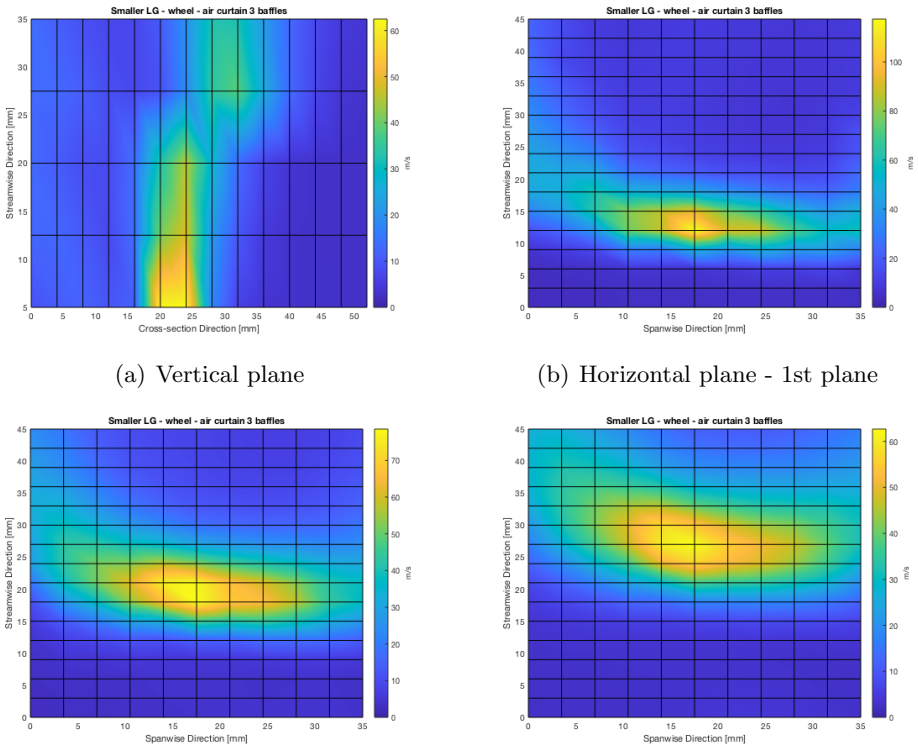

(a) Vertical plane

(b) Horizontal plane - 1st plane

(c) Horizontal plane - 2nd plane

(d) Horizontal plane - 3rd plane

Figure 5.4: Velocity contours of 4 study planes for the new short wheel air curtain, using HWA

conditions. According to the 2D velocity profile of the new profile (see Fig. 5.5(b)), the simulation highlighted some changes. First, the shielding height is greater, as well as the maximum velocity. The blue recirculation zone inside the air curtain in Fig. 5.5(a) has been removed; the flow seems to be coming straight out in Fig. 5.5(b). It is, however, difficult to see if there has been a change in the interaction of the outside shape with the cross-flow.

The second objective of the CFD analysis was to check that numerical simulations gave similar results to those of the flow-velocity tests. In order to replicate similar conditions, velocity contours were plotted at the same distance as the planes presented above. Results are shown in Fig. 5.6 and Fig. 5.7. Compared to the results of the hot-wire tests, velocity profiles are similar in distribution, although lower in magnitudes. They have the same crescent shape and condensed higher velocities, which become lower as the test planes get further away from the air curtain. In the third horizontal plane (Fig. 5.6(e)), the crescent is not distinct anymore, the air velocities smudge, and the flow velocity is greatly decreased. The vertical plane results, shown in Fig. 5.7(a), can be compared to both the 2D Ansys results, and the hot-wire results. The experimental results are similar to those calculated during the 3D

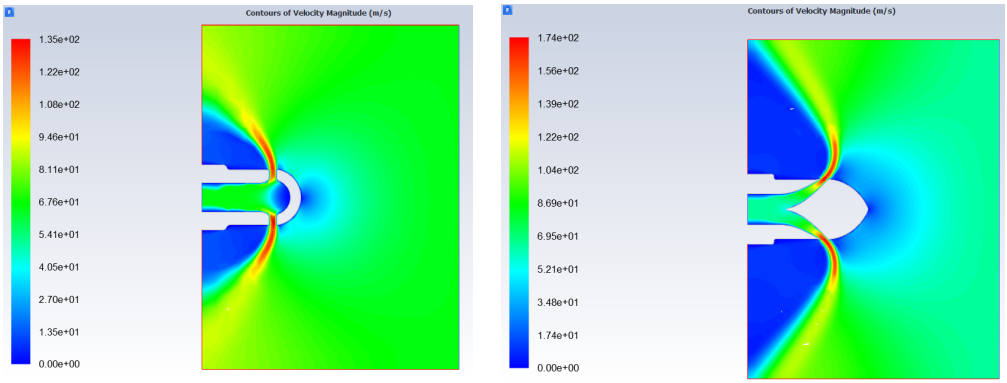

(a) Baseline design (b) New design

Figure 5.5: Comparison of 2D velocity profiles on Ansys Fluent: baseline design from the preliminary tests, and new design for the short wheel air curtain

simulation: the air comes out at an angle, as seen previously. We see again the decrease in velocity and the smudge at lower velocities. While experimental and numerical tests cannot really be compared in terms of velocity magnitudes, 2D and 3D CFD results show a pattern: the velocity magnitudes in 2D analysis are higher than those of the 3D.

The 3D analysis also allowed measures that were not possible using the hot-wire probe. Fig. 5.8 shows a close-up of the flow exiting the air curtain, by plotting a velocity contour tangent to the geometry. This velocity contours shows that the air coming out of the air curtain doesn't have a homogeneous velocity within the same opening. Velocity is higher in the central openings, as seen previously, but is also higher on the upper side of the openings. The same is visible for the external openings, with higher velocity towards the top. The top or the upper side refer to the side opposite the inlet side.

5.1.3 Discussion

A first redesign was done with this short wheel air curtain with baffles. The modification of the cavities inside the air curtain and the introduction of baffles gave new results in both numerical and experimental tests.

The utilisation of baffles seems to bring a new flow velocity distribution, with high velocities coming out of the air curtain's centre. This heterogeneity spanwise is undesired and the next design should look at bringing more of the central flow to the sides of the air curtain.

The noise issue has not be resolved by getting rid of the inner chamber. The 2D Ansys analysis shows however that the slow "blue" zone in the precedent air curtain has disappeared. There can be two explanations: either the "blue" zone is not recirculation and doesn't gen-

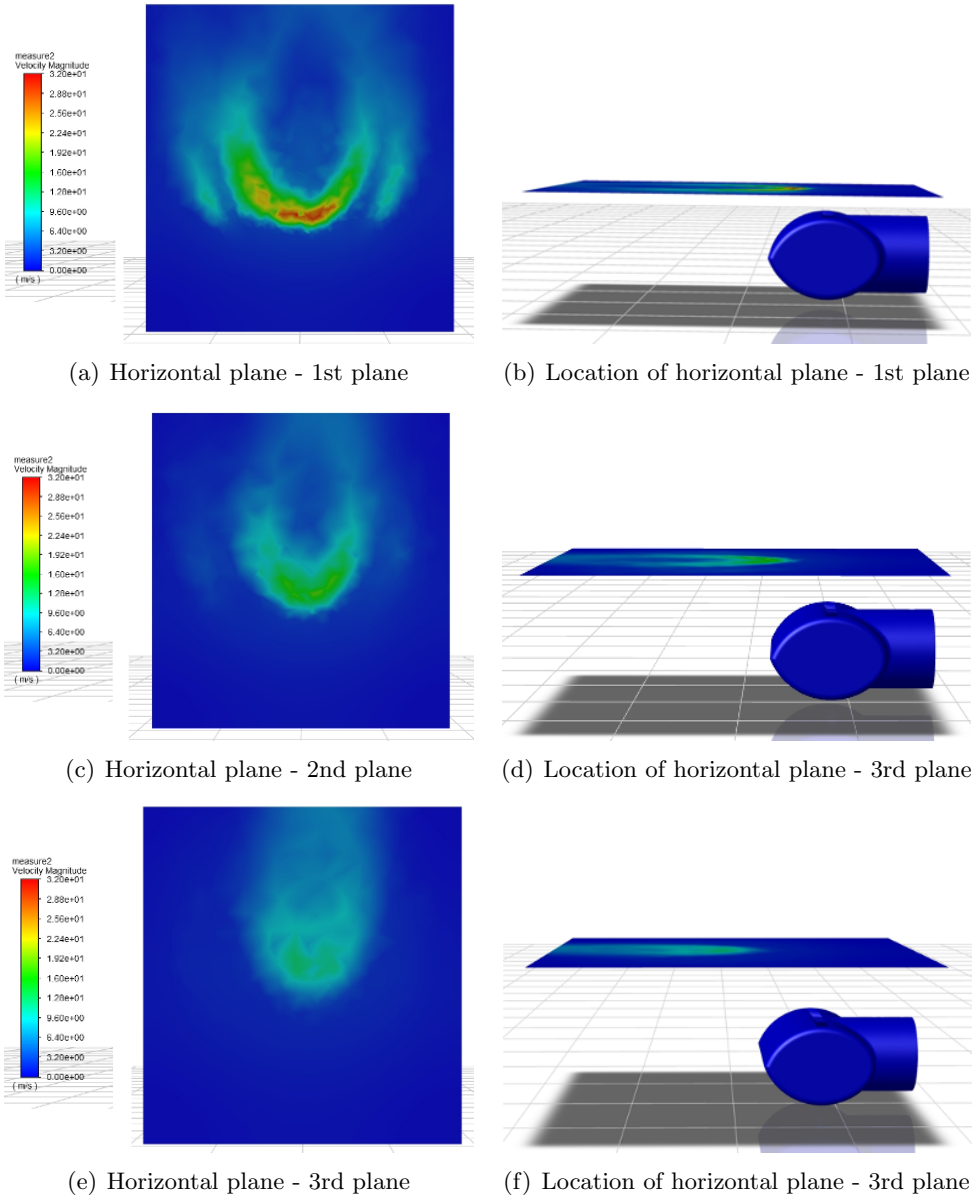

(a) Horizontal plane - 1st plane

(b) Location of horizontal plane - 1st plane

(c) Horizontal plane - 2nd plane

(d) Location of horizontal plane - 3rd plane

(e) Horizontal plane - 3rd plane

(f) Location of horizontal plane - 3rd plane

Figure 5.6: Velocity contours of horizontal study planes for the new short wheel air curtain, using Ansys Fluent

erate noise, or else there are still more significant noise sources that need to be discovered and countered.

The last 3D Ansys analysis also underlines a potential heterogeneity in the flow distribution within an opening, with more flow coming out at the side opposite the flow inlet. This could be explained by the flow trajectory inside the air curtain; the flow comes in the air curtain horizontally and follows the internal curvature to leave the air curtain at an angle. Because this happens over a short distance, the angle gradient is high and could result in the

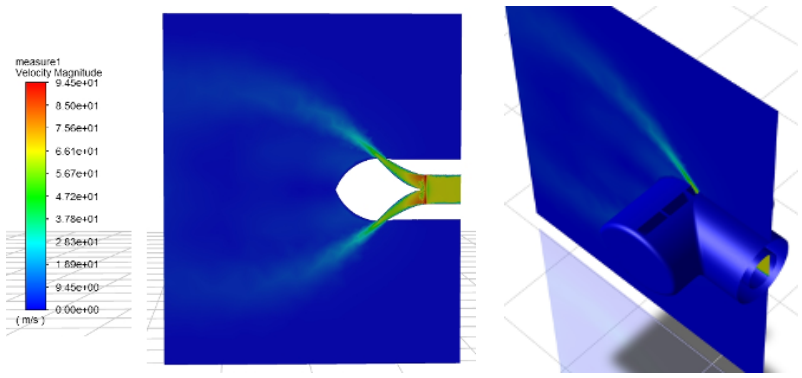

(a) Vertical plane (b) Location of vertical plane

Figure 5.7: Velocity contours of vertical study plane for the new short wheel air curtain, using Ansys Fluent

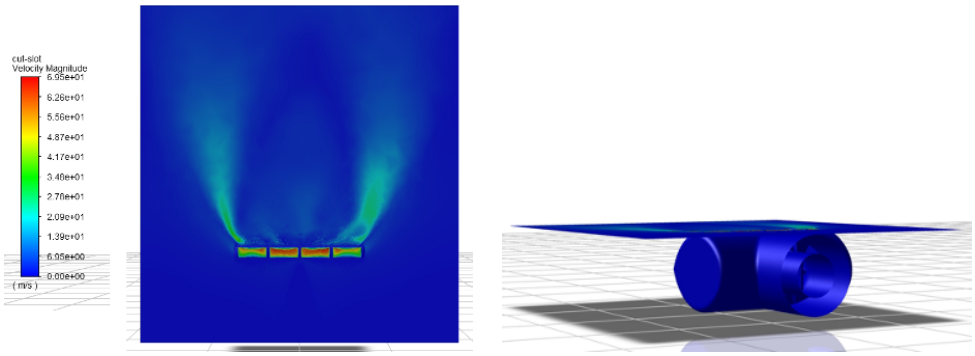

(a) Closer view (b) Location of closer view

Figure 5.8: Velocity contours of closer study plane for the new air curtain, using Ansys Fluent

air sticking to the wall it is projected against. In the same way, the central air injection is divided by the baffles and parts of the flow are quickly directed to the extremities, inducing a sharp turn in the stream. The steep redirections could have an effect on the flow distribution. In the next design, an effort should be made to lessen the gradients, and hopefully get a more homogeneous flow coming out of the air curtain.

Once again, it's important to note that the velocities from the hot-wire measurements should not be considered as absolute. Ansys analysis can be compared to previous results both in terms of velocity magnitude and distribution, as same boundary conditions were used. With these tests, numerical analysis shows that velocity magnitudes are different when doing the 2D or the 3D analysis. Only the 3D analysis accounts for the difference in section area between the entrance and exit of one of the air curtain's streams. It is for this reason that

velocity magnitudes for the flow coming out of the air curtains are lower in 3D analysis than in 2D analysis.

In the next design, modifications should be done on the design to lessen the gradients in the inner streams, to direct more of the flow to the sides and to reduce the noise.

5.2 Long wheel air curtain with baffles

This last section studies the redesign a long wheel air curtain. The new geometry is presented, as well as results the experimental tests and CFD analysis. They are compared with results from the previous designs and discussed in a final section.

5.2.1 Air curtain geometry

When the other designs focused on a short wheel air curtain, this redesign is centred on a long wheel air curtain with baffles for the smaller assembly. Its objective is to shield the wheel link as well as the wheels themselves. The choice of working on a long wheel air curtain in this final design is due to the wish to lessen the angle gradients while redirecting the flow. A longer air curtain allows for a gentler redirection of the flow, both from the centre to the extremities (using baffles), and from the centre to the openings. Other changes are:

- The existing baffles are starting closer to the flow entrance to increase the length of each separate stream and have the redirection happen over a longer distance;
- More baffles were added further down the streams to redivide the flow and hopefully bring it to the extremities of the air curtain;
- All geometries in contact with the flow have fillets (baffles, openings). This could help reduce disturbance as the flow hits those geometries;
- The outside shape facing the cross-flow has been changed to a NACA 0013 foil. This should help reduce the sound of the air curtain in a cross-flow, as this kind of geometry has been designed by the NASA to be implemented in high cross-flows (airplanes, F1 cars...).

The resulting design is presented in Fig. 5.9. Fig. 5.10 provides a section view of the baffles and the different streams within the air curtain.

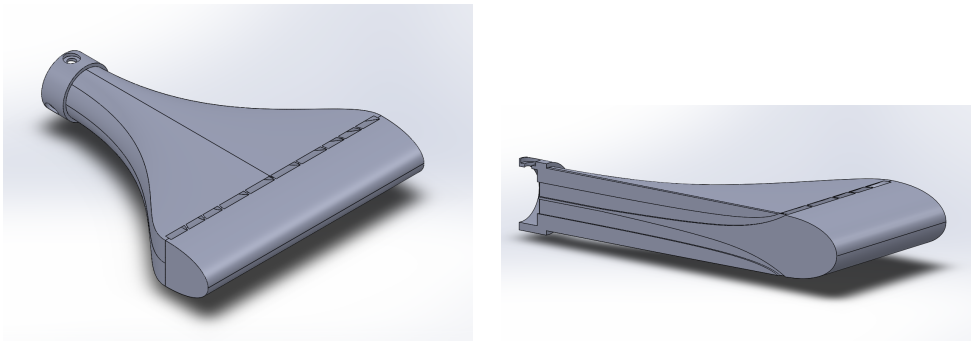

(a) Isometric view (b) Section view

Figure 5.9: New design for the 3rd cycle

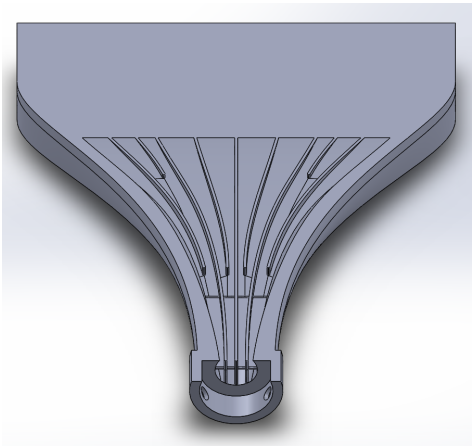

Figure 5.10: Section view of 3rd design with flow division using baffles

5.2.2 Adapter geometry

The previous short wheel air curtain with baffles still generated significant noise, even though the recirculation zone had been removed by the change of design. In an effort to remove all potential noise sources, attention was given to the adapter used to connect the air curtain to the air-supplying hose during tests. Its initial design is presented in Fig. 5.11(a). The upper part is inserted inside the hose, and the holes in the lower part receive brass inserts to allow the air curtain to be screwed on.

Two changes were made to hopefully enhance the adapter's performance:

- The brass inserts were cut and filed to avoid them sticking out in the internal flow, see Fig. 5.12(b);
- The transition from the hose internal diameter to the adapter internal diameter was made smoother by adding a fillet, see Fig. 5.11(b).

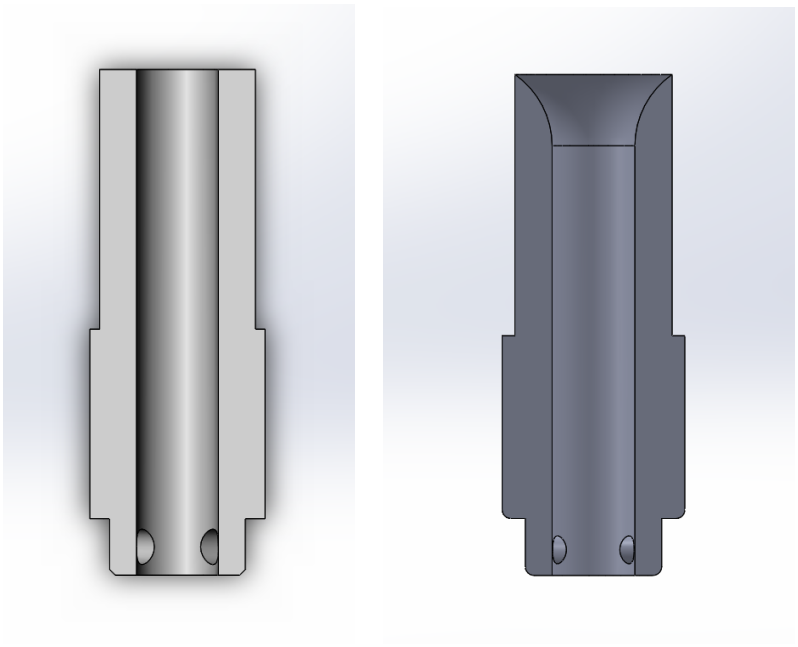

(a) Old adapter (b) New adapter

Figure 5.11: Changes in design for the hose adapter

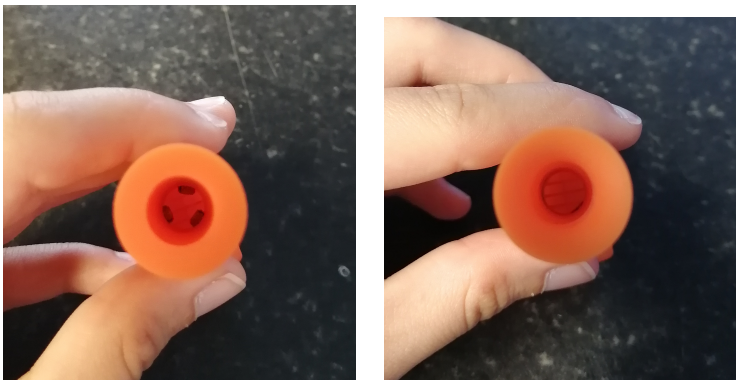

(a) Old adapter (b) New adapter with fillet and reduced brass inserts

Figure 5.12: Comparison of adapter designs

5.2.3 Results

Preemptive CFD analysis

For this design, the CFD analysis was performed before printing the air curtain, to ensure a first validation and to avoid making multiple prints. The 2D analysis, shown in Fig. 5.13, revealed a unexpected behaviour. In a quiescent environment, the air doesn't exit the air curtain following the stream's curvature, but sticks to the outside NACA shape. In a cross-flow, the CFD analysis does not converge to a solution, despite a higher number of iterations

and a finer mesh. This behaviour is not desirable in this case, as we want the exiting flow to separate from the air curtain to form a shield in a cross-flow. The design was modified and different exiting angles were tested, changing the slope of the stream. By making 5° steps, the first suitable results were obtained for the 65° air curtain design, shown in Fig. 5.14. With this design, the exiting flow was separating correctly in a quiescent environment, as well as forming shields for both medium and high velocity cross-flows. The initial design and the final design are shown in Fig. 5.15.

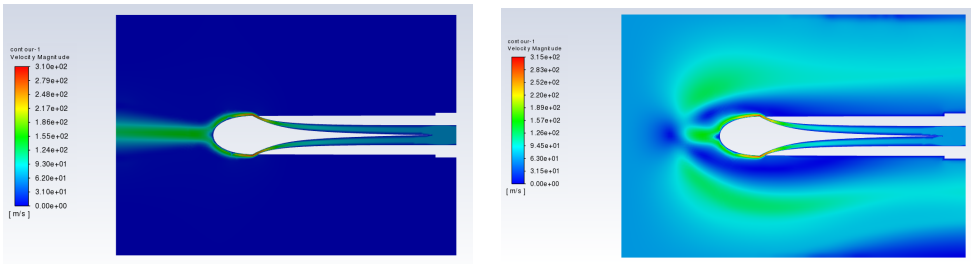

(a) 30° - 2D analysis - No cross-flow (b) 30° - 2D analysis - 65 m/s cross-flow

Figure 5.13: 2D Ansys analysis of flow with a 30° outlet angle

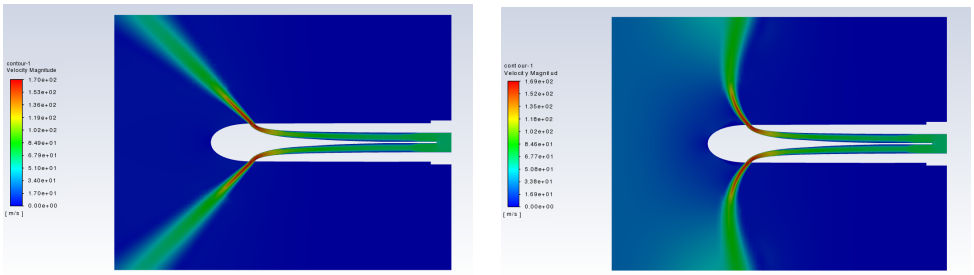

(a) 65° - 2D analysis - No cross-flow (b) 65° - 2D analysis - 30 m/s cross-flow

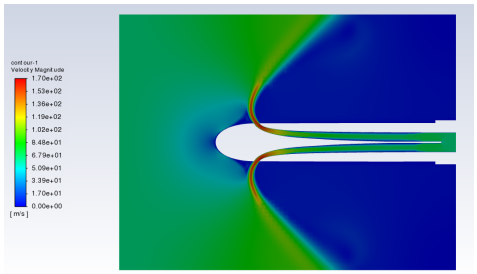

(c) 65° - 2D analysis - 65 m/s

Figure 5.14: 2D Ansys analysis of flow with a 65° outlet angle

The 65° version was then printed, tested and compared to other designs, both in terms of velocities and sound levels.

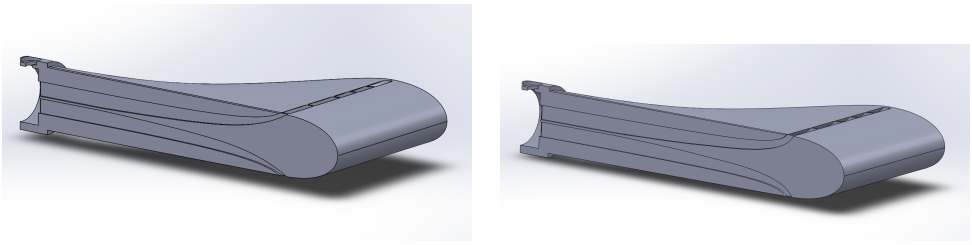

(a) 30° design (b) 65° design

Figure 5.15: Comparison of section views: 30° inclined outlet, and 65° inclined outlet

Sound-level tests

3 geometries went through sound-level tests and flow-velocity tests, and results were compared. The 3 geometries are:

- The short wheel air curtain for the smaller landing gear, presented in Section 4.1, referred to as the "baseline" air curtain;
- The short wheel air curtain for the smaller landing gear, presented in Section 5.1.1, referred to as the "short" air curtain;
- The long wheel air curtain for the smaller landing gear, presented in Section 5.2.1, referred to as the "long" air curtain;

For these measures, the air curtains blew air at medium speed (tank valve half-opened) and high speed (tank valve fully opened). The results of the fully-opened valve are shown in Fig. 5.16, the half-opened results, as well as the raw values, can be found in Annex F.

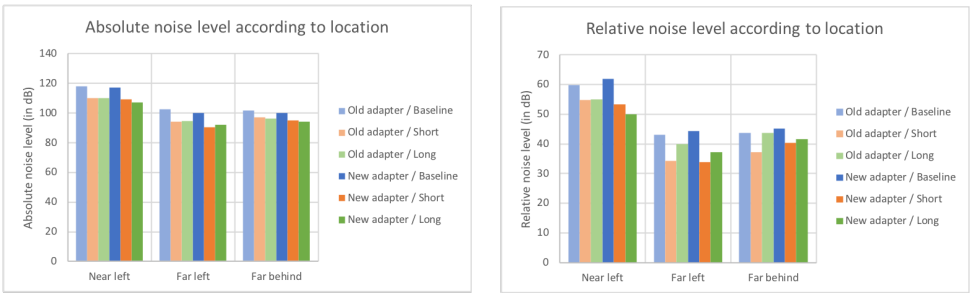

(a) Absolute noise level (b) Relative noise level

Figure 5.16: Noise levels depending on the air curtain and the adapter for different locations of the meter (see Fig. 3.3) - high flow

Results shown in Fig. 5.16 can be described as follows:

- The relative noise levels clearly underline the fact that the air curtains were important noise sources during tests, sometimes increasing the ambient noise by over 60 dB. The absolute noise values reached harmful levels and the use of ear protections was absolutely necessary;
- The baseline air curtain was always louder than the other geometries, regardless of the adapter used;
- The short and long air curtains did not have significantly different performances during the two tests with medium and high flow;
- The high flow tests did not show a clear reduction in noise level with the use of the new adapter. However, such trend can be seen in the medium flow results, see Fig. F.1.

Flow-velocity tests

Sound-level tests required to control the self-noise induced by the air curtains, but they needed to be complemented by an analysis of the flow, to ensure that the air curtains still have their shielding capability.

In a final test, the flow velocity coming out of the air curtains was measured to check if it was sufficient enough and if the distribution was homogeneous. The values were taken along the plane described in Fig. 5.3(b). Results for the high flow are shown in Fig. 5.17. Results for the medium flow are shown in Appendix G.

By comparing the velocity profiles plotted in Fig. 5.17, several things can be noted:

- All air curtains combined with the new adapter have a similar or lower peak velocity. Both the baseline and the short air curtains used with the new adapter saw their peak velocity decreased by about 20 m/s;
- The velocities achieved with the new adapter are less concentrated and seem to form a more uniform air blade;
- The long air curtain has a significantly bigger section area for its openings, which results in a much lower flow velocity;
- The combined use of baffles and the new adapter seems to be redistributing the flow to the centre and the intermediate sections, but the flow still struggles to reach all the way to the extremities.

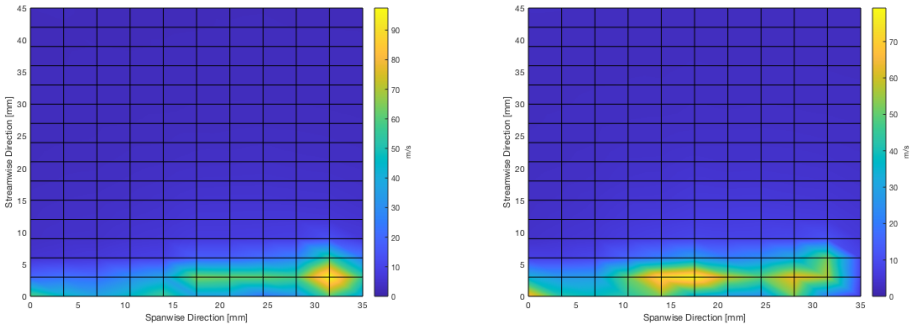

(a) Old adapter - Baseline AC

(b) New adapter - Baseline AC

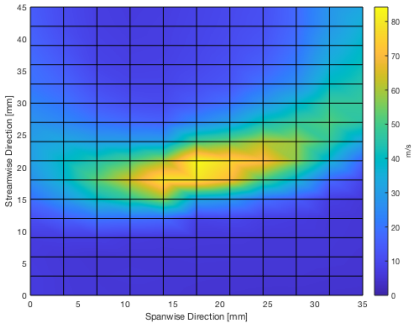

(c) Old adapter - Short AC

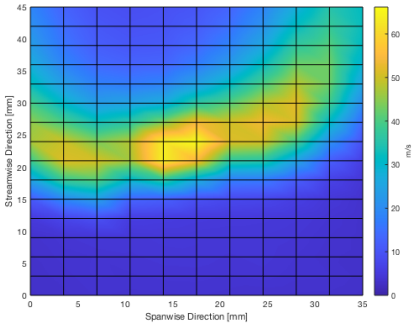

(d) New adapter - Short AC

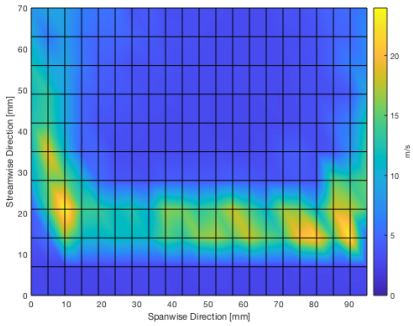

(e) Old adapter - Long AC

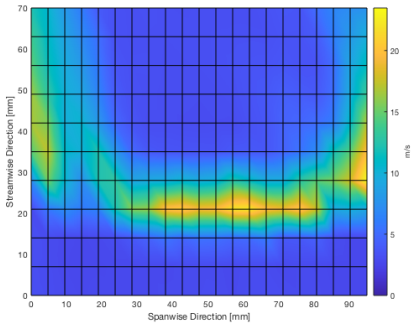

(f) New adapter - Long AC

Figure 5.17: Velocity profiles for different combinations of adapters and air curtains - high velocity, using HWA

5.2.4 Discussion

These results, which compare the main designs studied during the research project, give some insights on the performance of the air curtains.

From a flow velocity and distribution perspective, the new air curtains (short wheel and long wheel air curtains), combined with the new adapter, offered some progress. These combinations redistribute the flow more evenly, but reduce the peak velocity.

It is important to note that the "ambient" sound level measures varied by ± 5 dB for a similar ambient noise, which can impact the relative results. Because the sound level meter could not be calibrated, the absolute sound level measures give an approximate magnitude but keep all results proportional to one another. Knowing that, it can be concluded that there are still major issues with the noise generated by the air curtains. The new designs are less loud than the baseline air curtain but still produce too much noise.

It is also important to underline that the short wheel and long wheel air curtains cannot really be compared in terms of flow velocity, because of the difference in openings' section areas. However, because of the low flow velocity coming out of the long wheel air curtain, one could have expected less noise. Because there is no significant difference between the short wheel and long wheel air curtains in terms of sound level, the noise seems unrelated to the air coming out of the air curtain, but could rather be related to parts that are similar between the two designs, such as the adapter, the connection between the adapter and the air curtain, as well as the first baffles.

5.3 Discussion

The initial results agreed with previous studies, where air curtains can be loud and a great source of self noise, but can also shelter bluff bodies and reduce noise at certain frequencies, if designed correctly.

Preliminary results, from both experimental and numerical tests, rapidly gave ideas for a better performance with the removal of the "chamber" to avoid flow recirculation and reduce the noise, and the addition of baffles to guide the flow and homogenise its distribution.

Results for the redesigned air curtains and adapters were encouraging, because the new air curtains managed, in the end, to globally lower their self-noise levels and to distribute the flow more evenly, at the cost of a small decrease in peak flow velocity.

Efforts should be made to increase the measurements' accuracy but tests, both numerical and experimental (noise level and hot-wire), were conducted with identical tools, coefficients and boundary conditions, and can therefore be compared to one another.

Chapter 6

Conclusions

6.1 Introduction

This research project focused on the use of air curtains to reduce the noise generated by landing gear. Air curtains are potential low-noise technologies, with the advantages of having a small volume, being relatively light and unobtrusive (allowing visual checks). Tests were performed on newly designed and 3D-printed air curtains, mounted on scaled landing gear, and tested in cross-flow or quiescent conditions. Their performances were experimentally monitored using noise level tests, and hot-wire anemometry to check flow velocities and flow distributions. Flow interactions with the air curtains were also regularly computed using the CFD analysis software Ansys Fluent.

Air curtains can reduce specific noise

A test in Germany revealed that a modified torque link air curtain was able to shield a small rod, and therefore suppress a whistling sound at 4000 Hz. This test reaffirmed the air curtain's capability to reduce noise, if correctly designed.

Air curtains still generate a lot of self-noise, but redesign has lowered the noise level

The designs developed during this research project were still very loud, generating self-noise in quiescent conditions. The level of noise was however decreased when air recirculation was limited in the last 2 designs.

The adapter impacts the flow velocity and distribution

The use of the new adapter reduced the peak velocity achieved by the air curtains, but also resulted in a more homogeneous flow velocity exiting the central/intermediate openings. The extremities of the air curtains still lack some flow velocity.

Air curtains with same inlet conditions but different outlet conditions have same noise level

The long wheel air curtain and the short wheel air curtain had similar noise levels and different flow velocities. This seems to point that the inlet conditions could be the source of the noise generated by both air curtains, since a change of outlet conditions had little to no impact on the noise level.

6.2 Future work

According to the findings listed above, this research project could be continued in order to achieve a quieter air curtain.

One area of improvement could be the mechanical connection between the adapter and the air curtain. The current geometries are fragile and the use of brass inserts is not optimal. In order to avoid all possible leaks, a modified air curtain could be bolted on a modified adapter, without holes or screws sticking into the flow. The bolted assembly could also allow for the use of a ring seal, further increasing the airthightness.

Another possibility to explore in a future design could be the location of the baffles in the air inlet. Baffles are currently regularly spaced, but their locations could take into account the flow velocity profile coming out of the adapter, and be modified to change the section area between each baffle and to reach an equal flow rate. This could help bring more flow the air curtains' extremities.

Finally, the modified torque link air curtain used in Germany to suppress the whistling sound could be thoroughly studied in TCD's test conditions to better understand why it was able to reduce this particular noise. It would also be interesting to see how the two new designs would perform in DLR's wind tunnel during similar tests. This would provide a very useful comparison.

Bibliography

[1] W. Dobrzynski. Almost 40 years of airframe noise research: What did we achieve? *Journal of Aircraft*, 47(2):353–367, 2010. ISSN 0021-8669. doi: 10.2514/1.44457.

[2] Mitsuhiro Murayama, Yuzuru Yokokawa, Kazuomi Yamamoto, and Tohru Hirai. Computational study of low-noise fairings around tire-axle region of a two-wheel main landing gear. *Computers & Fluids*, 85:114–124, October 2013. ISSN 00457930. doi: 10.1016/j.compfluid.2012.11.001. URL https://linkinghub.elsevier.com/retrieve/pii/S004579301200429X.

[3] R. Elkoby, L. Brusniak, R.W. Stoker, M.R. Khorrami, A. Abeysinghe, and J.W. Moe. Airframe noise results from the QTD II flight test program. 2007. ISBN 978-1-62410-003-1.

[4] Kun Zhao, Sajad Alimohammadi, Patrick N. Okolo, John Kennedy, and Gareth J. Bennett. Aerodynamic noise reduction using dual-jet planar air curtains. *Journal of Sound and Vibration*, 432:192–212, October 2018. ISSN 0022460X. doi: 10.1016/j.jsv.2018.06.036. URL https://linkinghub.elsevier.com/retrieve/pii/S0022460X18303985.

[5] Jasper Wickerhoff and Tjaard Sijpkes. Aeroplane provided with noise-reducing means, as well as a landing gear and blowing means, June 2004. URL https://patents.google.com/patent/US20040104301/en.

[6] Airline industry worldwide - number of flights 2004-2022, . URL https://www.statista.com/statistics/564769/airline-industry-number-of-flights/.

[7] Union des Aéroports Français, . URL https://www.aeroport.fr/view-statistiques/beauvais-tille.

[8] R. Sordello, O. Ratel, F.F. de Lachapelle, C. Leger, A. Dambry, and S. Vanpeene. Evidence of the impact of noise pollution on biodiversity: A systematic map. *Environmental Evidence*, 9(1), 2020. ISSN 2047-2382. doi: 10.1186/s13750-020-00202-y.

[9] A.L. Brown. Measuring the effect of aircraft noise on sea birds. *Environment International*, 16(4-6):587–592, 1990. ISSN 0160-4120. doi: 10.1016/0160-4120(90)90029-6.

[10] M. Basner, C. Clark, A. Hansell, J. Hileman, S. Janssen, K. Shepherd, and V. Sparrow. Aviation Noise Impacts: State of the Science. *Noise and Health*, 19(87):41–50, 2017. ISSN 1463-1741. doi: 10.4103/nah.NAH-104-16.

[11] D.S. Lee, D.W. Fahey, P.M. Forster, P.J. Newton, R.C.N. Wit, L.L. Lim, B. Owen, and R. Sausen. Aviation and global climate change in the 21st century. *Atmospheric Environment*, 43(22-23):3520–3537, 2009. ISSN 1352-2310. doi: 10.1016/j.atmosenv.2009.04.024.

[12] Environmental Noise Guidelines, . URL `https://www.euro.who.int/en/health-topics/environment-and-health/noise/environmental-noise-guidelines-for-the-european-region`.

[13] C. Clark and K. Paunovic. Who environmental noise guidelines for the European region: A systematic review on environmental noise and quality of life, wellbeing and mental health. *International Journal of Environmental Research and Public Health*, 15(11), 2018. ISSN 1661-7827. doi: 10.3390/ijerph15112400.

[14] M. Basner and S. McGuire. WHO environmental noise guidelines for the european region: A systematic review on environmental noise and effects on sleep. *International Journal of Environmental Research and Public Health*, 15(3), 2018. ISSN 1661-7827. doi: 10.3390/ijerph15030519.

[15] T. Münzel, M. Sørensen, and A. Daiber. Transportation noise pollution and cardiovascular disease. *Nature Reviews Cardiology*, 18(9):619–636, 2021. ISSN 1759-5002. doi: 10.1038/s41569-021-00532-5.

[16] C. Baudin, M. Lefèvre, P. Champelovier, J. Lambert, B. Laumon, and A.-S. Evrard. Self-rated health status in relation to aircraft noise exposure, noise annoyance or noise sensitivity: the results of a cross-sectional study in France. *BMC Public Health*, 21(1), 2021. ISSN 1471-2458. doi: 10.1186/s12889-020-10138-0.

[17] Charles Stuart. Low Carbon Transport Technology, Power Sources - Gas Turbines, 2021.

[18] Kun Zhao, Patrick Okolo, Eleonora Neri, Peng Chen, John Kennedy, and Gareth J. Bennett. Noise reduction technologies for aircraft landing gear-A bibliographic review. *Progress in Aerospace Sciences*, 112:100589, January 2020. ISSN 03760421. doi: 10.1016/j.paerosci.2019.100589. URL https://linkinghub.elsevier.com/retrieve/pii/S0376042119300338.

[19] Kun Zhao, Xi-xiang Yang, Patrick N Okolo, Wei-hua Zhang, and Gareth J. Bennett. Use of a plane jet for flow-induced noise reduction of tandem rods. *Chinese Physics B*, 25(6):064301–1 – 064301–9, June 2016. ISSN 1674-1056. doi: 10.1088/1674-1056/25/6/064301. URL http://stacks.iop.org/1674-1056/25/i=6/a=064301?key=crossref.b90e51e4f1a72600400a9f694ec0b0af.

[20] Kun Zhao, Patrick N. Okolo, Yong Wang, John Kennedy, and Gareth J. Bennett. An Experimental Characterization of the Interaction Between Two Tandem Planar Jets in a Crossflow. *Journal of Fluids Engineering*, 140(11):111106–1 – 111106–12, June 2018. ISSN 0098-2202. doi: 10.1115/1.4040224. URL http://fluidsengineering.asmedigitalcollection.asme.org/article.aspx?doi=10.1115/1.4040224.

[21] INVENTOR (Webpage). . URL https://w3.onera.fr/inventor/home.

[22] M.J.T. Smith and K.W. Bushell. Turbine noise its significance in the civil aircraft noise problem. volume 1969-January, 1969. ISBN 978-0-7918-8005-0. doi: 10.1115/69WA/GT12.

[23] Joseph R. Crotti. The Role of State Government in Aircraft Noise Abatement Regulation. *SAE Transactions*, 80:1406–1410, January 1971. ISSN 0096736X. URL https://elib.tcd.ie/login?url=https://search.ebscohost.com/login.aspx?direct=true&db=edsjsr&AN=edsjsr.44737836. Publisher: Society of Automotive Engineers, Inc.

[24] Jan Böttcher. Noise Certification Workshop - ICAO, October 2004.

[25] Effective Perceived Noise Level - an overview | ScienceDirect Topics, . URL https://www.sciencedirect.com/topics/engineering/effective-perceived-noise-level.

[26] Ascent, . URL https://ascent.aero/.

[27] Lillian Gipson. AATT Technical Challenges, April 2016. URL http://www.nasa.gov/aeroresearch/programs/aavp/aatt/technical-challenges.

[28] Protecting the environment and the energy supply | Acare, . URL https://www.acare4europe.org/sria/flightpath-2050-goals/protecting-environment-and-energy-supply-0.

[29] P.O.A.L. Davies, M.J. Fisher, and M.J. Barratt. The characteristics of the turbulence in the mixing region of a round jet. *Journal of Fluid Mechanics*, 15(3):337–367, 1963. ISSN 0022-1120. doi: 10.1017/S0022112063000306.

[30] Donald Bartlett. THE EFFECTS OF USING NOISE REDUCTION TURBOFAN ENGINE NOZZLE DESIGNS ON A TURBOJET ENGINE. 1:12, 2016.

[31] Leonard Lopes and Casey Burley. Design of the Next Generation Aircraft Noise Prediction Program: ANOPP2. June 2011. doi: 10.2514/6.2011-2854.

[32] N. Molin, J.-F. Piet, L.C. Chow, M. Smith, W.M. Dobrzynski, and C. Seror. Prediction of low noise aircraft landing gears and comparison with test results. volume 5, pages 2878–2887, 2006. ISBN 978-1-56347-809-3.

[33] Martin R Fink. AIRFRAME NOISE PREDICTION METHOD. *Federal Aviation Administration*, page 141, March 1977.

[34] Y. Guo. A semi-empirical model for aircraft landing gear noise prediction. volume 5, pages 2912–2930, 2006. ISBN 978-1-56347-809-3. doi: 10.2514/6.2006-2627.

[35] N. Molin. Airframe noise modeling and prediction. *CEAS Aeronautical Journal*, 10(1): 11–29, 2019. ISSN 1869-5582. doi: 10.1007/s13272-019-00375-4.

[36] G. Romani and D. Casalino. Rotorcraft blade-vortex interaction noise prediction using the Lattice-Boltzmann method. *Aerospace Science and Technology*, 88:147–157, 2019. ISSN 1270-9638. doi: 10.1016/j.ast.2019.03.029.

[37] S. Satcunanathan, M.H. Meinke, and W. Schröder. Prediction of noise mitigation by porous media based on a direct-hybrid CFD/CAA method. 2019. ISBN 978-1-62410-588-3. doi: 10.2514/6.2019-2696.

[38] D. Casalino, A.F.P. Ribeiro, E. Fares, and S. Nölting. Lattice-Boltzmann aeroacoustic analysis of the LAGOON landing-gear configuration. *AIAA Journal*, 52(6):1232–1248, 2014. ISSN 0001-1452. doi: 10.2514/1.J052365.

[39] Hans Henrik Bruun. *Hot-wire anemometry: principles and signal analysis*. OUP Oxford, 1995. ISBN 0-19-856342-6.

[40] Y. Yang, Y. Liu, R. Liu, C. Shen, P. Zhang, R. Wei, X. Liu, and P. Xu. Design, validation, and benchmark tests of the aeroacoustic wind tunnel in SUSTech. *Applied Acoustics*, 175, 2021. ISSN 0003-682X. doi: 10.1016/j.apacoust.2020.107847.

[41] J. Kompenhans, M. Raffel, L. Dieterle, T. Dewhirst, H. Vollmers, K. Ehrenfried, C. Willert, K. Pengel, C. Kähler, A. Schröder, and O. Ronneberger. Particle Image Velocimetry in Aerodynamics: Technology and Applications in Wind Tunnels. *Journal of Visualization*, 2(3-4):229–244, 2000. ISSN 1343-8875. doi: 10.1007/BF03181440.

[42] Kun Zhao, Patrick N. Okolo, John Kennedy, and Gareth J. Bennett. 2D PIV measurement on the interaction zone between two parallel planar jets in a crossflow. *AIP Advances*, 7(10):105104, October 2017. doi: 10.1063/1.5005017. URL `http://aip.scitation.org/doi/abs/10.1063/1.5005017`.

[43] R. Merino-Martínez, J. Kennedy, and G.J. Bennett. Experimental study of realistic low–noise technologies applied to a full–scale nose landing gear. *Aerospace Science and Technology*, 113, 2021. ISSN 1270-9638. doi: 10.1016/j.ast.2021.106705.

[44] Kun Zhao, Patrick N Okolo, John Kennedy, and Gareth J Bennett. A study of planar jet flow control and perforated fairings for the reduction of the flow-induced noise of tandem rods in a cross-flow (AIAA2016-2772). Lyon, France, May 2016. AIAA. doi: 10.2514/6.2016-2772. URL `http://arc.aiaa.org/doi/10.2514/6.2016-2772`.

[45] Kun Zhao, Yong Liang, Patrick N. Okolo, Yong Wang, Zeping Wu, and Gareth J. Bennett. Suppression of aerodynamic noise using dual-jet air curtains combined with perforated fairings. *Applied Acoustics*, 158:107042, January 2020. ISSN 0003682X. doi: 10.1016/j.apacoust.2019.107042. URL `https://linkinghub.elsevier.com/retrieve/pii/S0003682X19301793`.

[46] Stefan Oerlemans and Anton de Bruin. Reduction of Landing Gear Noise Using an Air Curtain. In *15th AIAA/CEAS Aeroacoustics Conference (30th AIAA Aeroacoustics Conference)*, Miami, Florida, May 2009. American Institute of Aeronautics and Astronautics. ISBN 978-1-60086-967-9. doi: 10.2514/6.2009-3156. URL `http://arc.aiaa.org/doi/abs/10.2514/6.2009-3156`.

[47] Gareth J. Bennett, Jiang Lai, Gordon O'Brien, Daniele Ragni, Francesco Avallone, and Michael Pott-Pollenske. Flow Control and Passive Low Noise Technologies for Landing Gear Noise Reduction. In *28th AIAA/CEAS Aeroacoustics 2022 Conference*, Southampton, UK, June 2022. American Institute of Aeronautics and Astronautics. ISBN 978-1-62410-664-4. doi: 10.2514/6.2022-2848. URL `https://arc.aiaa.org/doi/10.2514/6.2022-2848`.

Appendix A

Additional pictures of the hot-wire-anemometry set-up

Figure A.1: Valve under the sink (open), allowing the compressed air tank to fill up

Figure A.2: Tank valve (open), allowing the compressed air to flow in the system

Figure A.3: Mass flow meter, removed for test, to be connected to the tank and to the chamber during calibration

Figure A.4: Tank-to-chamber configuration during hot-wire anemometry tests

Figure A.5: Orange hot-wire probe holder or grey hot-wire probe holder to maintain the probe above the opening (grey hose to be removed for calibration)

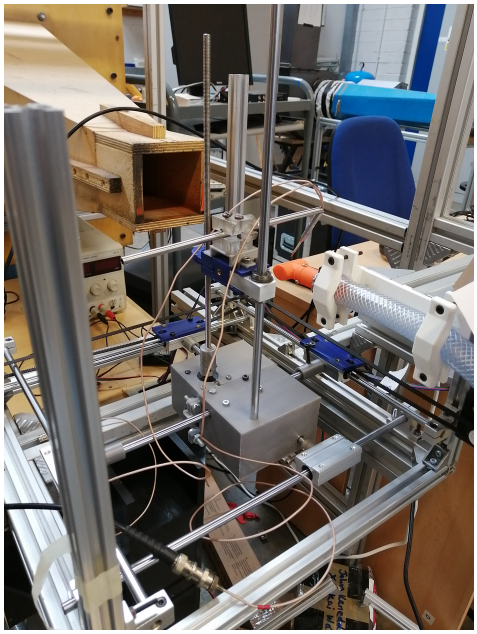

Figure A.6: Traverse with air curtain (orange) on the right and hot-wire probe mounted on CNC holder in the centre

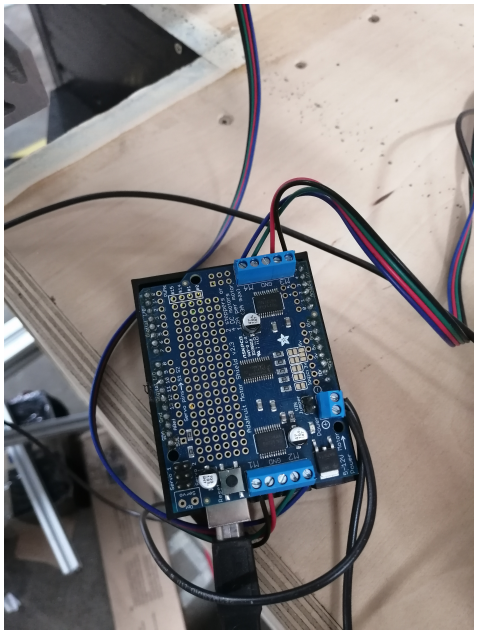

Figure A.7: Arduino board used to activate the stepper motors

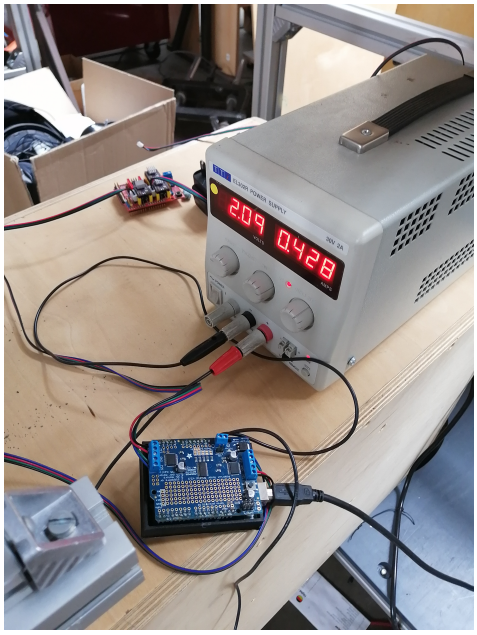

Figure A.8: Generator used to power the motors via the Arduino board

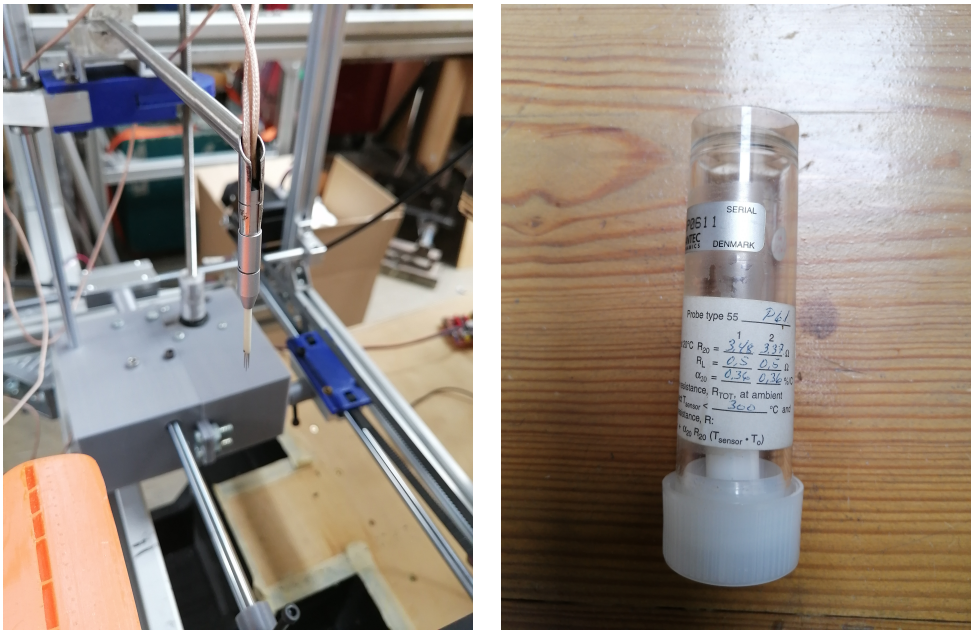

(a) Probe (b) Probe casing

Figure A.9: Probe used for hot-wire tests

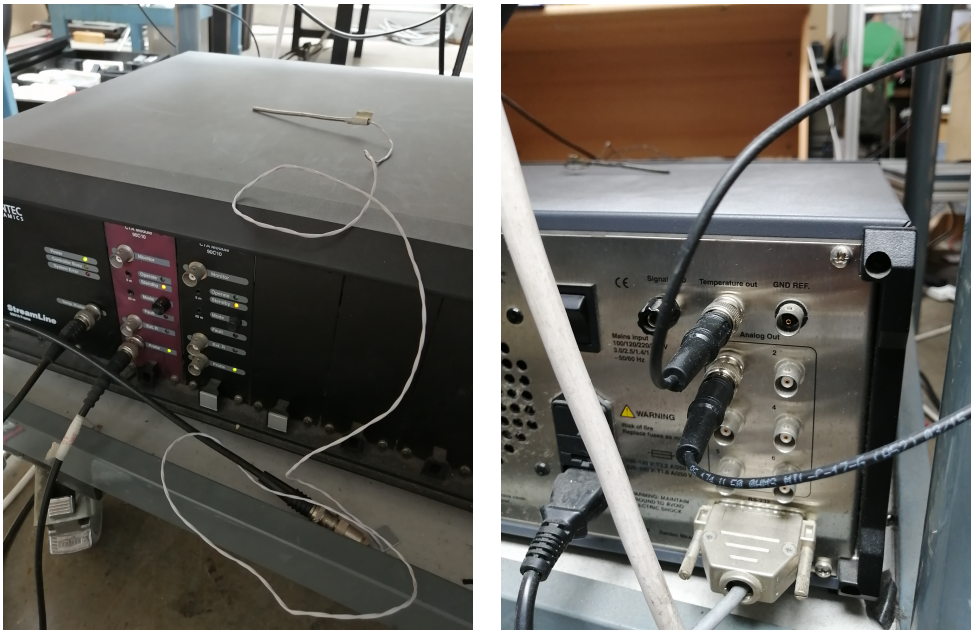

(a) Front (b) Back

Figure A.10: StreamLine frame connected to the hot-wire probe, a temperature probe (front), the computer and the PXI-1033 controller (back)

Figure A.11: Connections on the PXI-1033 controller

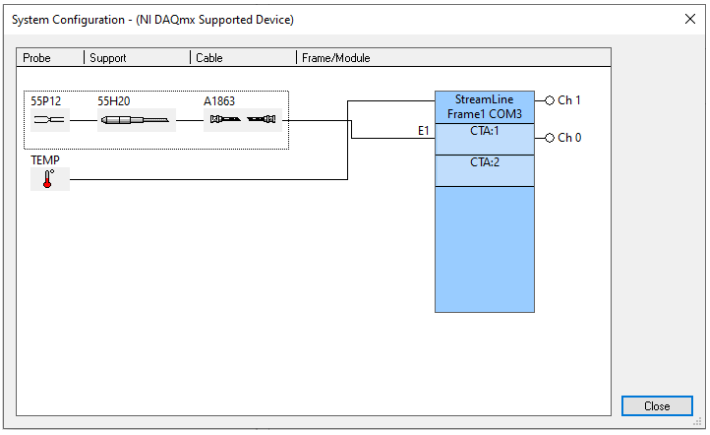

Figure A.12: Virtual replica of the set-up on the StreamWare software

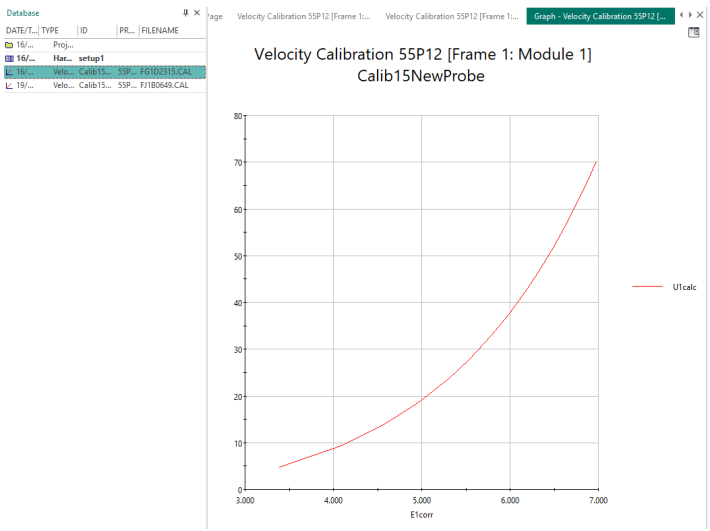

Figure A.13: Calibration curve: calculated flow velocity plotted against the corrected voltage

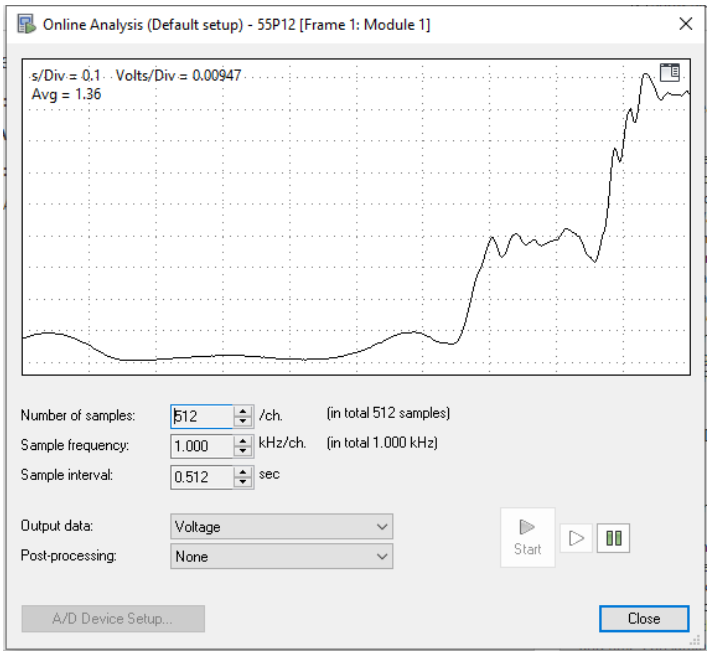

Figure A.14: Example of an online measure run, necessary to set the frame and the probe to “operate” mode

Appendix B

Matlab code for hot-wire-anemometry data acquisition and visualisation

B.1 Simple probe movement

```
close all;
clear all;
%%
%help daq

%% Defining motor control
a = arduino('COM4','Uno','Libraries','Adafruit/MotorShieldV2');
shield = addon(a,'Adafruit/MotorShieldV2');
smX = stepper(shield,1,200,'RPM',75);
smY = stepper(shield,2,200,'RPM',75);

%port 1 for X axis and 2 for Y
%X negative = away from tunnel
%Y negative = downwards motion
%50 steps per 10 mm for X axis i.e. 5 steps/mm
%2000 steps per 10 mm for Y axis i.e. 200 steps/mm

%   move(smX,-225);
%   move(smY,500);
%   move(smX,15);
%   move(smY,1000);
release(smX); %sometimes release is important and allows for a smoother ...
    movement
release(smY);
```

B.2 Data acquisition

```
close all;
clear all;
%% Verification of connection
daq.getVendors;
daq.getDevices;
%% Verification of probe operation
tic % start timer
daq.getDevices;
s=daq.createSession('ni'); %create national instrument session
addAnalogInputChannel(s,'PXI2Slot2',0,'Voltage');
s.Rate=1000; %1kHz frequency i.e. 1000 scans per second
s.NumberOfScans=5000; %5 seconds at each point for mean values

mesureU=s.startForeground();
moyenne=mean(mesureU); %to calculate mean values at each point
toc % end timer

%% Defining motor control
a = arduino('COM4','Uno','Libraries','Adafruit/MotorShieldV2');
shield = addon(a,'Adafruit/MotorShieldV2');
smX = stepper(shield,1,200,'RPM',75);
smY = stepper(shield,2,200,'RPM',75);

```

```
% Data acquisition

% change number of measure points if needed
tic % start timer
m=16;  %line Y axis
n=11;  % column X axis

C0=45.308; %calibration coefficients from streamware
C1=-42.997;
C2=15.114;
C3=-2.2777;
C4=0.153;

P=[C4 C3 C2 C1 C0]; %defining polynomial of coefficients

resultat1=zeros([m,n]);
voltage1=zeros([m,n]);
RMS=zeros([m,n]);
mesureU=[];
Tot=m*n;



daq.getDevices;
s=daq.createSession('ni');
addAnalogInputChannel(s,'PXI2Slot2',0,'Voltage');
s.Rate=1000;
s.NumberOfScans=5000;
disp('Starting movement')
pause(1)



%port 1 for X axis and 2 for Y
%X negative = away from tunnel
%Y negative = downwards motion
%50 steps per 10 mm for X axis i.e. 5 steps/mm
%2000 steps per 10 mm for Y axis i.e. 200 steps/mm


%change distance between points, and + or - depending on direction/stepper
%motor
for i=1:1:n   %line by line filling
    if mod(i,2)==0   %if even line i.e. L2 or L4 --> move downwards
        for j=1:1:m
            lig=m-j+1;   %filling by the end of the line
            mesureU=abs(s.startForeground());
            mesureVelocity=polyval(P,mesureU); % y = polyval(p,x) ...
                evaluates the polynomial p at each point in x.
            moy=mean(mesureU);
            moyenne=mean(mesureVelocity); %taking avg of all readings ...
                taken at that point
            R=mesureVelocity-moyenne;
            val=sqrt(mean(R.^2)); %finding rms value
            voltage1(lig,i)=moy;
            resultat1(lig,i)=moyenne
            RMS(lig,i)=val;
            Tot=Tot-1
            move(smX,-15);
            pause(0.5)
```

```
82          end
83          move(smX,15);
84          pause(1);
85          release(smX);
86          release(smY);
87          move(smY,-18)
88      else %if n is odd i.e. L1 or L3 --> move upwards
89          for j=1:1:m
90              mesureU=s.startForeground();
91              mesureVelocity=polyval(P,mesureU);
92              moy=mean(mesureU);
93              moyenne=mean(mesureVelocity);
94              R=mesureVelocity-moyenne;
95              val=sqrt(mean(R.^2))
96              voltage1(j,i)=moy;
97              resultat1(j,i)=moyenne
98              RMS(j,i)=val;
99              Tot=Tot-1
100             move(smX,15);
101             pause(0.5)
102         end
103         move(smX,-15);
104         pause(1);
105         release(smX);
106         release(smY);
107         move(smY,-18);
108     end
109     disp('Axis Changing')
110     pause(1)
111 end
112
113
114 toc % end timer
115 %%
116 % save('cyl_43_large_spacing_mean_velocity_porous','M');
117 % save('cyl_43_large_spacing_RMS_velocity_porous','RMS')
```

B.3 Data visualisation

```
1  close all;
2  clear all;
3
4
5  load('NewAdapter_3AC_10mmV2.mat','resultat1');%load results
6
7  [m,n]=size(resultat1);
8  % m number of lines (spanwise discretisation)
9  % n number of columns (streamwise discretisation)
10
11
12 dm=7; %distance between measure points on the Y axis
13 dn=4.75; %distance between measure points on the X axis
14
15 x=(0:dn:dn*(n-1)+0); %change 0 to value of offset if there is one
16 X=ones(m,n).*x;
```

```
17
18 y=(0:dm:dm*(m-1)+0); %change 0 to value of offset if there is one
19 Y=y'.*ones(m,n);
20
21
22 %To plot the measures' locations
23 % plot(X,Y,'r*')
24
25 %To get the maximum velocity achieved
26 % Max=max(resultat1);
27 % max=max(Max)
28
29 %To plot the velocity contour
30 visual=pcolor(X,Y,resultat1);
31 visual.FaceColor = 'interp';
32 c=colorbar;
33 cmax=max(caxis);
34 caxis([0,cmax])
35 c.Label.String = 'm/s';
36
37 ylabel('Streamwise Direction [mm]')
38 xlabel('Spanwise Direction [mm]')
39 title('Old Adapter - 3rd AC - 10mm above')
```

Appendix C

Additional pictures of the sound-level-test set-up

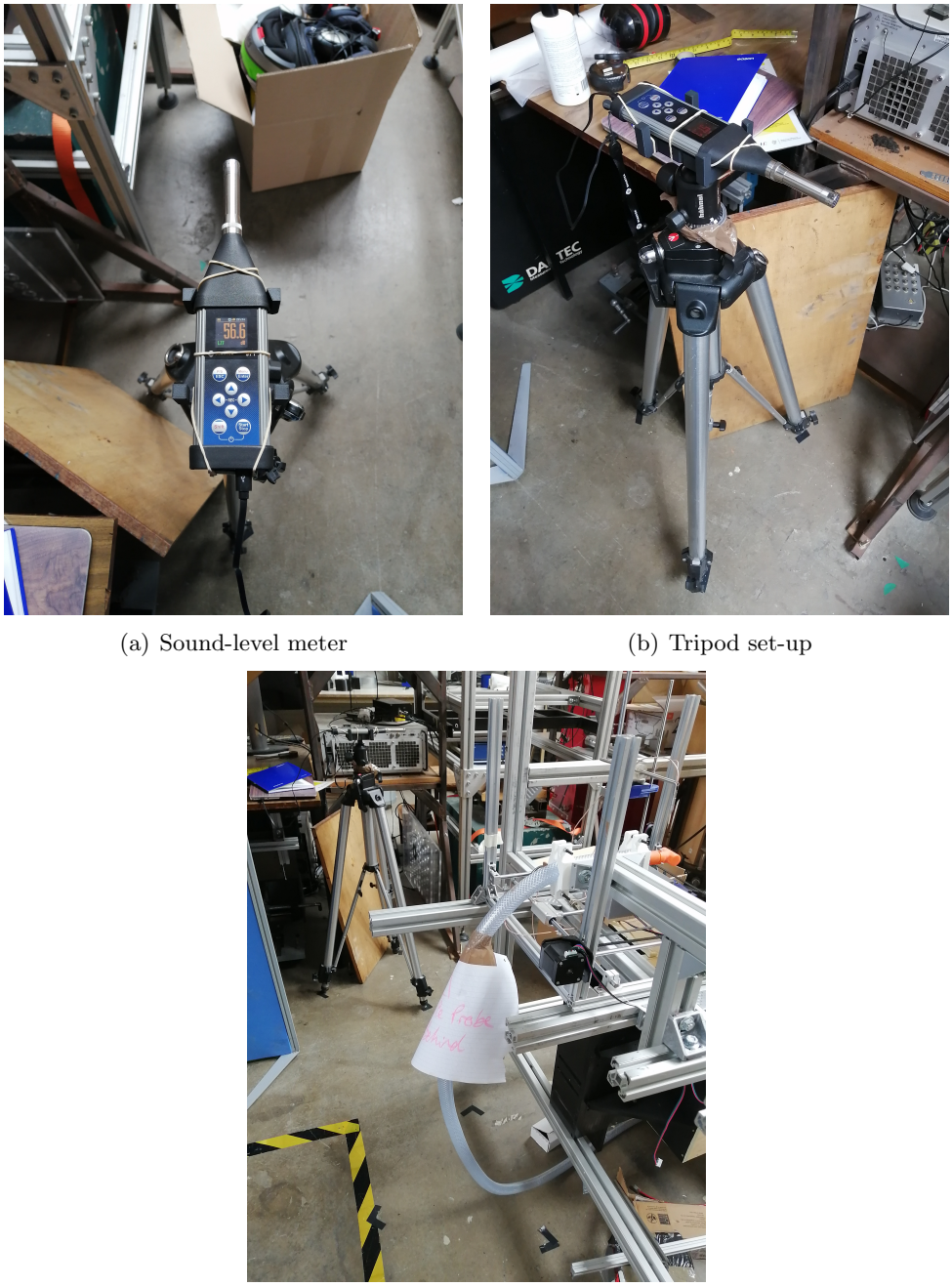

(a) Sound-level meter

(b) Tripod set-up

(c) Location relative to the air curtain

Figure C.1: Sound-level meter placed on a tripod with marking on the ground for the “Far left” and “Near left” location

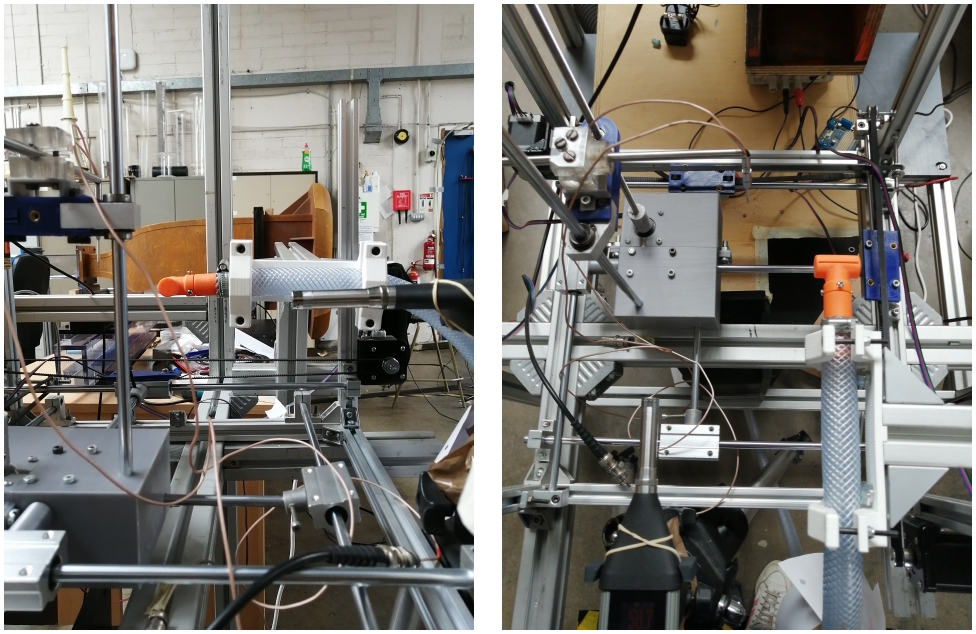

(a) Height of the SLM compared to the AC (b) Distance of the SLM compared to the AC

Figure C.2: Location of the SLM in the "Near left" configuration

Appendix D

Plane discretisation for flow-velocity tests - preliminary geometries

Each preliminary air curtain geometry undergoing a hot-wire flow velocity test is tested along a plane at discrete points. The data-acquisition locations are plotted in the following graphs, for each geometry.

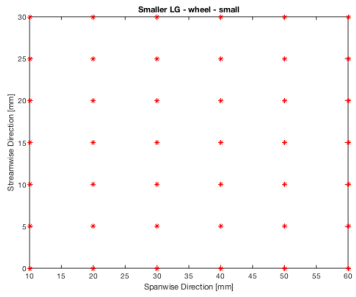

(a) Smaller landing gear - wheel - short

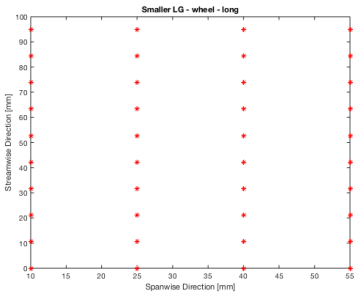

(b) Smaller landing gear - wheel - long

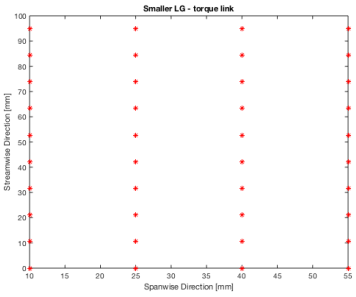

(c) Smaller landing gear - torque link

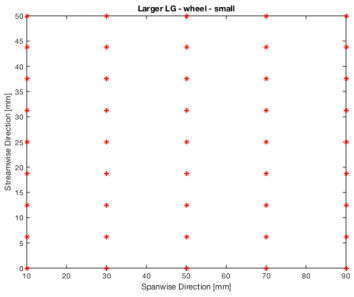

(d) Larger air curtain - wheel - short

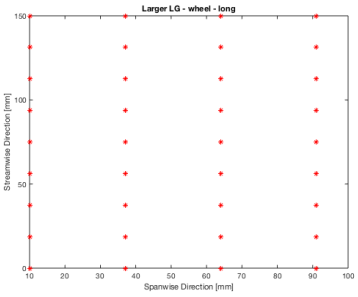

(e) Larger air curtain - wheel - long

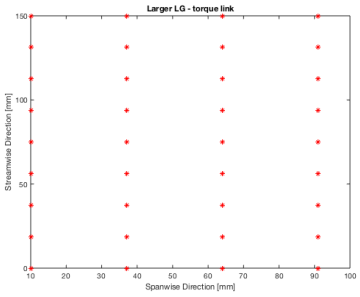

(f) Larger air curtain - torque link

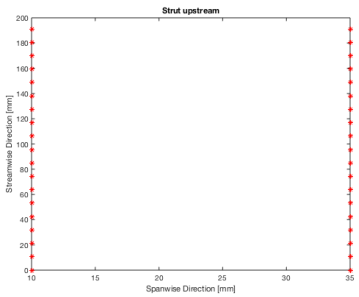

(g) Strut upstream

Figure D.1: Locations of test points

Appendix E

Velocity contours for other preliminary AC geometries

In Fig. E.1, the flow coming out of a torque-link air curtain is plotted. The torque-link air curtain geometry is asymmetrical, with an air injection happening towards one extremity. The resulting profile is also asymmetrical, with most of the flow coming out of the extremity opposite the injection. The velocities are also lower than with the shorter air curtains.

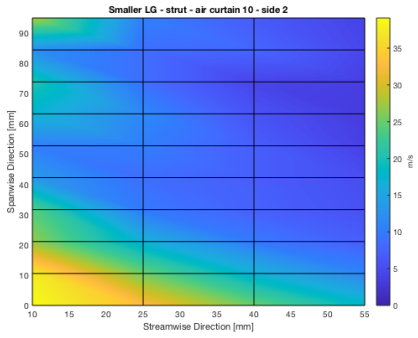

Figure E.1: Velocity profile exiting a torque-link air curtain, using HWA

The strut geometry was tested using hot-wire anemometry. While several geometry variations have been experimented, Fig. E.2 shows the velocity profile of an air curtain with two slit widths and two wall thicknesses. The results that stand out are: the velocity peak appearing when the slit/wall parameters change mid-height, and the highest peak being located at the top of the air curtain. It is not fully displayed in the contour, due to the limits of the traverse, but the highest velocity was actually situated above the air curtain, leading to a very heterogeneous distribution of the flow

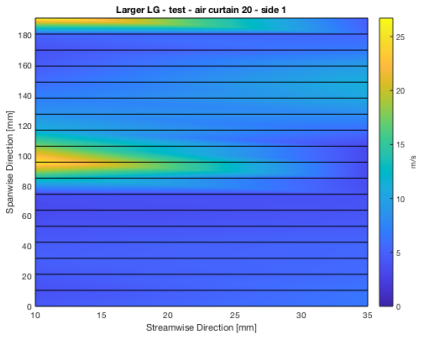

Figure E.2: Velocity profile exiting a strut air curtain, using HWA

Appendix F

Sound-level-test results

The measurement "Ambient" is a measurement taken when no air comes out of the air curtain. The measurement "Test" is a measurement taken when the air curtain is blowing air. The column "Difference" is calculated by subtracting the "Ambient" sound level to the "Test" sound level. The sound level "Difference" therefore represents the contribution of the air curtain to the noise measured during "Test". The locations are described in Fig. 3.3.

F.1 Results - medium flow

Table F.1: Old adapter and baseline air curtain - medium flow

	Ambient (dB)	Test (dB)	Difference (dB)
Near left	50.6	98.3	47.7
Far left	52.1	82.0	29.9
Far behind	52.8	83.7	30.9

Table F.2: Old adapter and short air curtain - medium flow

	Ambient (dB)	Test (dB)	Difference (dB)
Near left	59.2	96.3	37.1
Far left	56.5	81.7	25.2
Far behind	59.0	80.7	21.7

Table F.3: Old adapter and long air curtain - medium flow

	Ambient (dB)	Test (dB)	Difference (dB)
Near left	58.8	95.1	36.3
Far left	56.6	78.1	21.5
Far behind	57.9	79.6	21.7

Table F.4: New adapter and baseline air curtain - medium flow

	Ambient (dB)	Test (dB)	Difference (dB)
Near left	53.6	97.6	44.0
Far left	54.1	81.7	27.6
Far behind	54.1	83.0	28.9

Table F.5: New adapter and short air curtain - medium flow

	Ambient (dB)	Test (dB)	Difference (dB)
Near left	58.7	83.7	25.0
Far left	57.2	69.6	12.4
Far behind	59.2	69.3	10.1

Table F.6: New adapter and long air curtain - medium flow

	Ambient (dB)	Test (dB)	Difference (dB)
Near left	58.9	87.0	28.1
Far left	61.4	70.9	9.5
Far behind	60.8	71.7	10.9

F.2 Results - high flow

Table F.7: Old adapter and baseline air curtain - high flow

	Ambient (dB)	Test (dB)	Difference (dB)
Near left	58.3	118.2	59.9
Far left	59.4	102.5	43.1
Far behind	57.9	101.6	43.7

Table F.8: Old adapter and short air curtain - high flow

	Ambient (dB)	Test (dB)	Difference (dB)
Near left	55.2	110.1	54.9
Far left	60	94.2	34.2
Far behind	59.9	97.2	37.3

Table F.9: Old adapter and long air curtain - high flow

	Ambient (dB)	Test (dB)	Difference (dB)
Near left	55.1	110.1	55.0
Far left	54.6	94.5	39.9
Far behind	52.4	96.1	43.7

Table F.10: New adapter and baseline air curtain - high flow

	Ambient (dB)	Test (dB)	Difference (dB)
Near left	55.3	117.3	62.0
Far left	55.6	100.0	44.4
Far behind	54.8	99.9	45.1

Table F.11: New adapter and short air curtain - high flow

	Ambient (dB)	Test (dB)	Difference (dB)
Near left	55.8	109.1	53.3
Far left	56.6	90.4	33.8
Far behind	54.7	95.1	40.4

Table F.12: New adapter and long air curtain - high flow

	Ambient (dB)	Test (dB)	Difference (dB)
Near left	57.4	107.3	49.9
Far left	54.6	91.9	37.3
Far behind	52.4	94.0	41.6

F.3 Result comparison - medium flow

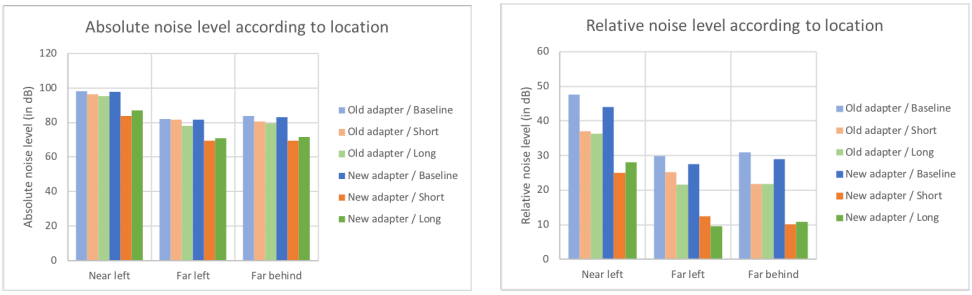

(a) Absolute noise level (b) Relative noise level

Figure F.1: Noise levels depending on the air curtain and the adapter for different locations of the meter (see Fig. 3.3) - medium flow

Appendix G

Velocity contours for main AC geometries - medium flow

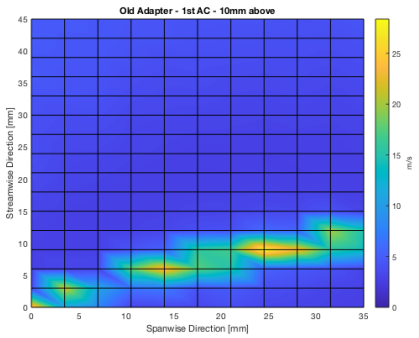

(a) Old adapter - Baseline AC

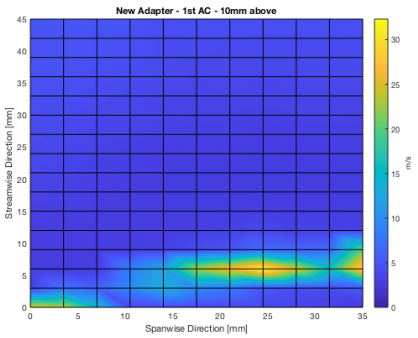

(b) New adapter - Baseline AC

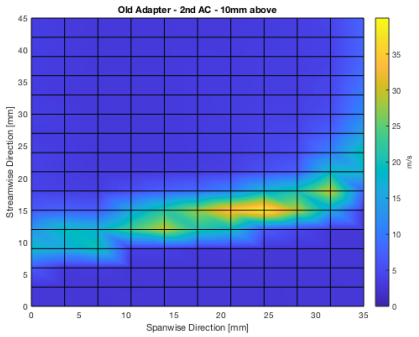

(c) Old adapter - Short AC

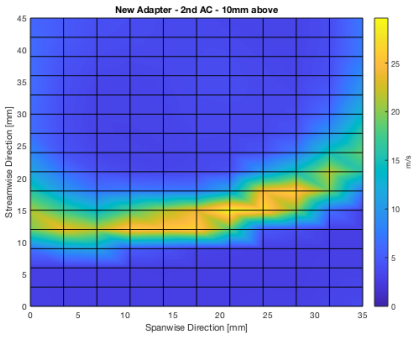

(d) New adapter - Short AC

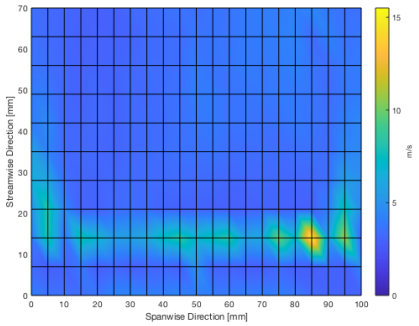

(e) Old adapter - Long AC

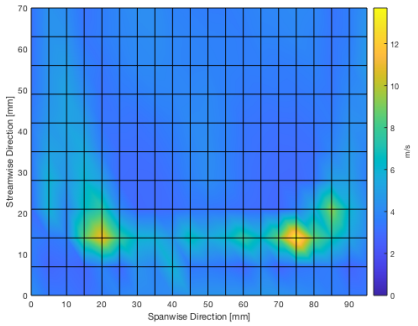

(f) New adapter - Long AC

Figure G.1: Velocity profiles for different combinations of adapters and air curtains - medium flow, using HWA